2021

Localization Chulalongkorn University of the infraorbital foramen and the accessory infraorbital foramen with reference to facial bony landmarks: the predicting method and its accuracy.

Jiraporn Suntiruamjairucksa
Faculty of Medicine

Localization of the infraorbital foramen and the accessory infraorbital foramen with reference to facial bony landmarks: the predicting method and its accuracy.

Miss Jiraporn Suntiruamjairucksa

A Thesis Submitted in Partial Fulfillment of the Requirements
for the Degree of Master of Science in Medical Sciences
Common Course
FACULTY OF MEDICINE
Chulalongkorn University
Academic Year 2021

การกำหนดตำแหน่งของรูใต้เบ้าตาและรูเสริมใต้เบ้าตาโดยใช้จุดสังเกตของกระดูกใบหน้าเป็นจุดอ้างอิง และความแม่นยำของวิธีการทำนายตำแหน่ง

น.ส.จิราภรณ์ สันติร่วมใจรักษ์

วิทยานิพนธ์นี้เป็นส่วนหนึ่งของการศึกษาตามหลักสูตรปริญญาวิทยาศาสตรมหาบัณฑิต
สาขาวิชาวิทยาศาสตร์การแพทย์ ไม่สังกัดภาควิชา/เทียบเท่า
คณะแพทยศาสตร์ จุฬาลงกรณ์มหาวิทยาลัย
ปีการศึกษา 2564

Thesis Title	Localization of the infraorbital foramen and the accessory infraorbital foramen with reference to facial bony landmarks: the predicting method and its accuracy.
By	Miss Jiraporn Suntiruamjairucksa
Field of Study	Medical Sciences
Thesis Advisor	Professor VILAI CHENTANEZ, M.D., Ph.D.

Accepted by the FACULTY OF MEDICINE, Chulalongkorn University in Partial Fulfillment of the Requirement for the Master of Science

..... Dean of the FACULTY OF MEDICINE
(Associate Professor CHANCHAI SITTIPUNT, M.D.)

THESIS COMMITTEE

..... Chairman
(Professor SITHIPORN AGTHONG, M.D., Ph.D.)

..... Thesis Advisor
(Professor VILAI CHENTANEZ, M.D., Ph.D.)

..... Examiner
(Assistant Professor DEPICHA JINDATIP, Ph.D.)

..... Examiner
(KRITSADA LEUNGCHAVAPHONGSE, M.D., Ph.D.)

..... External Examiner
(Assistant Professor Suwadee Chaunchaiyakul, Ph.D.)

จิราภรณ์ สันติร่วมใจรักษ์ : การกำหนดตำแหน่งของรูใต้เบ้าตาและรูเสริมใต้เบ้าตาโดยใช้จุดสังเกตของกระดูกใบหน้าเป็นจุดอ้างอิง และความแม่นยำของวิธีการทำนายตำแหน่ง. (Localization of the infraorbital foramen and the accessory infraorbital foramen with reference to facial bony landmarks: the predicting method and its accuracy.) อ.ที่ปรึกษาหลัก : ศ. ดร. แพทย์หญิงวิไล ชินธเนศ

การฉีดยาชาบริเวณเส้นประสาทใต้เบ้าตามีบทบาทในการระงับความรู้สึกบริเวณส่วนกลางของใบหน้า ดังนั้นตำแหน่งของรูใต้เบ้าตาและรูเสริมใต้เบ้าตาซึ่งเป็นทางออกของเส้นประสาท จึงมีความสำคัญ หลายการศึกษาหาตำแหน่งของรูทั้งสองนี้ แต่ผลการศึกษามีความแตกต่างกัน *วัตถุประสงค์* เพื่อทำนายตำแหน่งของรูใต้เบ้าตาและรูเสริมใต้เบ้าตา โดยใช้กระดูกจมูกส่วนหน้าและจุดต่ำสุดของบริเวณระหว่างกระดูกโหนกแก้มและกระดูกขากรรไกรบนเป็นจุดอ้างอิง (เส้น A) อธิบายความสัมพันธ์ของตำแหน่งระหว่างรูใต้เบ้าตาและรูเสริมใต้เบ้าตา และประเมินความแม่นยำของวิธีการทำนายตำแหน่ง *วิธีการ* ทำการศึกษาจาก 216 กะโหลก โดยวิเคราะห์ภายใต้กล้องจุลทรรศน์ใช้แสงแบบสเตอริโอ การหาตำแหน่งของรูใต้เบ้าตาจะทำการวัดระยะทางตั้งฉากจากรูใต้เบ้าตาลงมาที่เส้นอ้างอิง A (B) และหาอัตราส่วนของระยะทางจากกระดูกจมูกส่วนหน้าไปถึงจุดตัดของเส้น B กับเส้น A (D) ต่อระยะ A (D:A) หากพบรูเสริมใต้เบ้าตาในกะโหลกที่ศึกษา จะทำการวัดระยะต่างๆเช่นเดียวกัน การประเมินความแม่นยำของวิธีการทำนายตำแหน่งศึกษาจากร่างอาจารย์ใหญ่ 15 ร่าง โดยวัดระยะทางระหว่างรูที่ทำนายและรูที่พบจริง *ผลการศึกษา* พบรูเสริมใต้เบ้าตาทั้งหมด 86 รู โดยส่วนใหญ่อยู่ด้านบนและด้านในต่อรูใต้เบ้าตา ยกเว้น 3 รู ที่อยู่ด้านล่างและด้านนอกต่อรูใต้เบ้าตา การทำนายตำแหน่งของรูใต้เบ้าตาทำได้โดยใช้ระยะ B ซึ่งมีค่า 15.14 ± 1.99 มิลลิเมตร และอัตราส่วนระยะทาง D:A ซึ่งมีค่าเท่ากับ 63.35 ± 3.9% เช่นเดียวกันกับรูใต้เบ้าตา การหาตำแหน่งของรูเสริมใต้เบ้าตาใช้ระยะในแนวตั้งฉากคือ 19.34 ± 3.36 มิลลิเมตร และอัตราส่วนคือ 51.8 ± 5.9% การวิเคราะห์ทางสถิติพบว่า ไม่มีความแตกต่างกันอย่างมีนัยสำคัญทางสถิติของค่าเฉลี่ยในแต่ระยะทางระหว่างข้างและเพศของกะโหลก การศึกษาจากร่างอาจารย์ใหญ่พบว่า ตำแหน่งของรูใต้เบ้าตาที่ทำนายอยู่ด้านใต้และด้านนอกต่อรูที่ใต้เบ้าตาที่เจอจริง เป็นระยะเฉลี่ย 0.59 ± 1.39 และ 1.10 ± 1.44 มิลลิเมตร ซึ่งอาจไม่ส่งผลจากการคลำโดยใช้ปลายนิ้ว และรูใต้เบ้าตาที่ทำนายอยู่ตรงกับรูที่เจอจริงร้อยละ 50 ดังนั้นผลการศึกษานี้สามารถนำมาใช้เป็นแนวทางในการหาตำแหน่งของรูใต้เบ้าตาและรูเสริมใต้เบ้าตา และมีประโยชน์ในทางปฏิบัติ

สาขาวิชา วิทยาศาสตร์การแพทย์ ลายมือชื่อนิสิต .....

ปีการศึกษา 2564 ลายมือชื่อ อ.ที่ปรึกษาหลัก .....

6372002030 : MAJOR MEDICAL SCIENCES

KEYWORD: Accessory infraorbital foramen, Facial landmark, Infraorbital foramen, Localization, Predicting method

Jiraporn Suntiruamjairucksa : Localization of the infraorbital foramen and the accessory infraorbital foramen with reference to facial bony landmarks: the predicting method and its accuracy.. Advisor: Prof. VILAI CHENTANEZ, M.D., Ph.D.

The infraorbital nerve block is commonly used for mid-facial anesthesia. Therefore, the location of infraorbital foramen (IOF) and accessory infraorbital foramen (AIOF) where the nerve exits through is important. Although, many studies tried to identify the location of IOF and AIOF using bony and soft tissue landmarks, the results varied in each study. *Objectives* To determine the location of IOF and AIOF with reference to the line between anterior nasal spine (ANS) and the lowest point of the zygomaticomaxillary junction (Z) which is defined as line A, describe anatomical relationship between IOF and AIOF, and assess an accuracy of the proposed predicting method. *Methods* A total of 216 skulls were examined. Live images were analyzed under the stereoscopic microscope. For localization of IOF, the vertical distance from IOF to line A (B) and the mean ratio of the distance between ANS and the intersecting point of the vertical line from IOF with line A (D) to distance A were analyzed. If AIOF was identified, all distances were measured similar to IOF. To assess an accuracy of the predicting method, 15 cadavers were studied by measuring the distance error between the predicted and the real foramen. *Results* There were 86 AIOFs. Most of them located superomedial to IOF except for 3 AIOFs which located in the inferolateral position. The location of IOF was predicted by using the vertical line B which was 15.14 ± 1.99 mm and the mean ratio of distance D to distance A (D:A) which was 63.35 ± 3.9%. For localization of AIOF, the mean vertical distance was 19.34 ± 3.36 mm and the mean ratio was 51.8 ± 5.9%. No statistically significant difference was found between sex and sides. In cadavers, the mean distance error of the predicted IOF was 1.10 ± 1.44 mm lateral and 0.59 ± 1.39 mm inferior to the real IOF and there were 50% of the predicted IOFs that accurately located within the real IOF. Therefore, this study provides an alternative method for localization of IOF and AIOF which could be useful in clinical settings.

Field of Study:	Medical Sciences	Student's Signature .....
Academic Year:	2021	Advisor's Signature .....

ACKNOWLEDGEMENTS

การจัดทำวิทยานิพนธ์เรื่อง การกำหนดตำแหน่งของรูใต้เบ้าตาและรูเสริมใต้เบ้าตาโดยใช้จุดสังเกตของกระดูกใบหน้าเป็นจุดอ้างอิง และความแม่นยำของวิธีการทำนายตำแหน่ง สามารถดำเนินการจนสำเร็จลุล่วงไปได้ด้วยดี เนื่องจากได้รับความความอนุเคราะห์และสนับสนุนจากบุคคลหลายท่าน

ขอขอบพระคุณ ศาสตราจารย์ดร. แพทย์หญิงวิไล ชินธเนศ ที่กรุณาเป็นอาจารย์ที่ปรึกษา ให้คำแนะนำ ช่วยเหลือ และให้ความรู้อันเป็นประโยชน์ต่อการทำวิจัยเป็นอย่างยิ่ง ตลอดจนปรับปรุงแก้ไขข้อบกพร่องต่างๆ ด้วยความเอาใจใส่ ทำให้วิทยานิพนธ์ฉบับนี้มีความสมบูรณ์และสำเร็จได้ด้วยดี ผู้วิจัยตระหนักถึงความตั้งใจและทุ่มเทของอาจารย์ และขอขอบพระคุณเป็นอย่างสูงไว้ ณ ที่นี้

ขอขอบพระคุณ คณะกรรมการสอบวิทยานิพนธ์ ได้แก่ ศาสตราจารย์ดร.นพ.สิทธิพร แอกทอง ศาสตราจารย์ดร. แพทย์หญิงวิไล ชินธเนศ ผู้ช่วยศาสตราจารย์ดร.เดภิชา จินดาทิพย์ อาจารย์ดร.นพ. กฤษฎา เหลืองชวพงศ์ และผู้ช่วยศาสตราจารย์ดร.สุวดี ชวนไชยะกูล ผู้กรุณาสละเวลาในการให้คำแนะนำ และปรับปรุงวิทยานิพนธ์ฉบับนี้ให้มีความสมบูรณ์

ขอขอบพระคุณ คุณอทิตยา ร่วมวงศ์ เจ้าหน้าที่บริการวิทยาศาสตร์ รวมถึงเจ้าหน้าที่ประจำหน่วยศูนย์ฝึกผ่าตัด และบริษัทไลก้า คาเมร่า (ไทยแลนด์) จำกัด ผู้ให้ความอนุเคราะห์ในการจัดหาวัสดุอุปกรณ์ เครื่องมือ และสถานที่ในการทำวิจัย

ขอขอบพระคุณเจ้าของเอกสารและงานวิจัยทุกท่าน ที่ผู้วิจัยศึกษาค้นคว้าและนำมาอ้างอิงในการทำวิจัย ตลอดจนร่างอาจารย์ใหญ่ที่อุทิศร่างกายเพื่อการศึกษา จากภาควิชากายวิภาคศาสตร์ คณะแพทยศาสตร์ จุฬาลงกรณ์มหาวิทยาลัย ที่ทำให้งานวิจัยเล่มนี้สามารถเกิดขึ้นและสำเร็จลุล่วงได้

สุดท้ายนี้ ขอขอบพระคุณฝ่ายบัณฑิตศึกษา คณะแพทยศาสตร์ จุฬาลงกรณ์มหาวิทยาลัย ผู้สนับสนุนทุนการศึกษาในหลักสูตรวิทยาศาสตร์มหาบัณฑิต รวมถึงบิดา มารดา และครอบครัว ที่ให้ความช่วยเหลือและกำลังใจเป็นอย่างดีเสมอมา

ผู้วิจัยหวังเป็นอย่างยิ่งว่าวิทยานิพนธ์ฉบับนี้จะมีประโยชน์แก่ผู้ค้นคว้าและก่อให้เกิดคุณค่าทางการศึกษาต่อไป

Jiraporn Suntiruamjairucksa

TABLE OF CONTENTS

LIST OF TABLES

Page

LIST OF FIGURES

Page

LIST OF ABBREVIATIONS

2D = two dimensions

3D = three dimensions

A = distance from anterior nasal spine to the lowest point of the zygomaticomaxillary junction

AIOA = accessory infraorbital artery

AIOF = accessory infraorbital foramen

AION = accessory infraorbital nerve

ANS = anterior nasal spine (tip of the intermaxillary suture of the maxilla bone)

B = vertical distance from the middle-upper edge of IOF to line A

C = vertical distance from the middle-upper edge of AIOF to line A

CB = Cupid's bow

CBCT = cone-beam computed tomography

D = distance from anterior nasal spine to the intersecting point of the vertical line from IOF with line A

E = distance from anterior nasal spine to the intersecting point of the vertical line from AIOF with line A

EN = external nasal nerve

F = the shortest horizontal distance from the predicted IOF to the real IOF

FM = facial midline

G = the shortest vertical distance from the predicted IOF to the real IOF

H = the shortest horizontal distance from the predicted AIOF to the real AIOF

I = the shortest vertical distance from the predicted AIOF to the real AIOF

IN = internal nasal nerve

IOA = infraorbital artery

IOF = infraorbital foramen

ION = infraorbital nerve

IP = inferior palpebral nerve

IQR = interquartile range

L= lacrimal caruncle

LAS = Leica Application Suite

LC = lateral canthus

Lt = left

ML = medial limbus

n = number

Predicted D = average distance A of the cadaver multiplied with the average D:A (63.35%)

Predicted E = average distance A of the cadaver multiplied with the average E:A (51.8%)

PX = horizontal distance between the predicted IOF and the real AIOF

PY = vertical distance between the predicted IOF and the real AIOF

R = r = radius

Rt = right

SD = standard deviation

SLl = lateral branch of superior labial nerve

SLm = medial branch of superior labial nerve

SN = subnasal point

X = horizontal distance between IOF and AIOF

Y = vertical distance between IOF and AIOF

Z = the lowest point of the zygomaticomaxillary junction

d = acceptable error

σ = the population standard deviation

$z_{\alpha/2}$ = alpha level's z-score

¶ = median and interquartile range

* = statistically significant difference between groups

® = mean and standard error of mean

CHAPTER I

INTRODUCTION

Backgrounds and Rationales

The infraorbital nerve (ION) derives from the maxillary nerve and emerges from infraorbital foramen (IOF) on the maxilla bone (1). This nerve provides mid-facial sensation in the area of lower eyelids, lateral side of nose, nasal septum, and upper lip (2, 3). The ION block is used for regional anesthesia in many procedures including maxillofacial, eye, nose and dental surgeries (4-7). Moreover, it is beneficial in treating intractable infraorbital neuralgia (8, 9) and reducing postoperative pain (5, 10, 11).

The standard method for identifying the location of IOF to perform the ION block is palpating below infraorbital margin for 8–10 mm in the mid-pupillary plane (12). Although this method is simple and widely acceptable, there was a failure rate of 17% when performing the ION block by this method of IOF identification (13). This could be because performing this procedure needs experience and there is an anatomical variation of facial anatomy which makes it harder to identify the foramen. There is a variation of IOF called accessory infraorbital foramen (AIOF). AIOF mostly located in the superomedial position to IOF (14). It was also found that neurovascular structures emerging from AIOF, the accessory infraorbital nerve (AION) and artery (AIOA), were associated with structures from IOF (15). The presence of AIOF can explain anesthetic postoperative complications in patient who did not have the ION injury during the operation, and the failure of achieving midfacial numbness in patient underwent adequate ION block (15). Accordingly, the location of IOF and AIOF is important and should be considered when performing mid-facial procedures. Although, there were numerous anatomical landmarks used as reference points, some of them were not applicable in practice. Therefore, palpable landmarks on the cheek are introduced.

This study aims to determine the location of IOF and AIOF using palpable bony landmarks which are anterior nasal spine (ANS) and the lowest point of the zygomaticomaxillary junction (Z), describe anatomical relationship between IOF and AIOF and assess an accuracy of the proposed predicting method in cadaver.

Research Questions

Primary research questions

1. What is the location of IOF with reference to the line between ANS and the lowest point of the zygomaticomaxillary junction in dry skulls?
2. What is the prevalence of AIOF?
3. What is the location of AIOF with reference to the line between ANS and the lowest point of the zygomaticomaxillary junction in dry skulls?

Secondary research questions

1. What is the relationship between the location of IOF and AIOF?
2. Is there the statistical difference in the location of IOF and AIOF between sex and sides of skulls?
3. What is an accuracy of the predicted location of IOF and AIOF?

Research Objectives

1. To localize IOF with reference to the line between ANS and the lowest point of the zygomaticomaxillary junction in horizontal and vertical directions
2. To evaluate the existence and number of AIOF
3. To localize AIOF with reference to the line between ANS and the lowest point of the zygomaticomaxillary junction in horizontal and vertical directions
4. To find the relationship between the location of IOF and AIOF
5. To analyze the statistical difference in the location of IOF and AIOF between sex and sides of skulls
6. To measure the distance between the predicted and the real foramen in cadavers

Research Methodology

Research Design

Descriptive study

Sample Population

This study uses dry skulls and embalmed cadavers from the Department of Anatomy, Faculty of Medicine, Chulalongkorn University, Thailand

Inclusion Criteria

1. Adult human dry skulls and embalmed cadavers
2. Facial region of skulls and cadavers are completely preserved

Exclusion Criteria

1. Skulls with anatomical distortion of the maxilla, zygoma, nasal, sphenoid and temporal bone
2. Cadavers with the maxilla and orbital anatomical distortion

Risk and Investigator's Responsibility

No

Venue of the Study

Department of Anatomy, Faculty of Medicine, Chulalongkorn University

Conceptual Framework

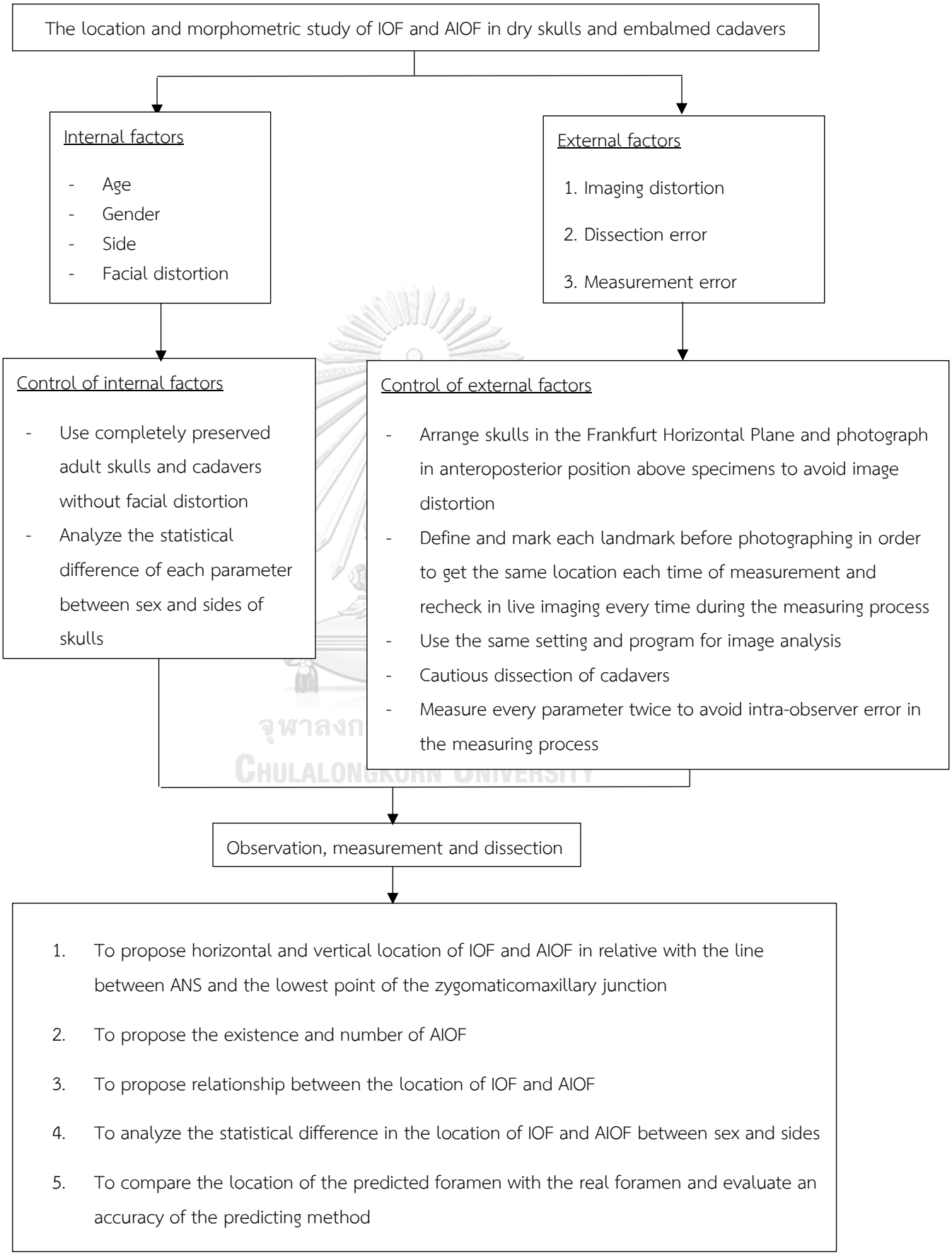

Data Analysis and Statistics

The statistical analysis is performed by SPSS software version 22.0 to calculate mean with standard deviation (SD) of each parameter, paired t-test analysis to assess the mean difference between the left and right side of specimens, independent t-test analysis to assess the mean difference between male and female specimens and linear regression analysis to evaluate the relationship between the location of IOF and AIOF. Intra-observer intraclass correlation coefficient is analyzed to assess the intra-observer reliability.

Ethical Consideration

Specimens used in this study are donated for anatomical study with respect to the right of donors in their own dead bodies. Cadavers and skulls are treated in respectful manner and with confidentiality. There is no mistreatment of the specimens and parts of the body that don't involve in this research are fully preserved. This study is approved by the Faculty of Medicine, Chulalongkorn University IRB committee (IRB no.698/64).

This cadaveric study can minimize potential risks to living patients and increase benefits by providing anatomical knowledge for clinical applications in performing surgical procedures.

Expected Benefits

This study provides new method for predicting the location of IOF and AIOF and explains anatomical information about the location and variation of AIOF. From this knowledge, clinicians can perform more effective and safer procedures around mid-facial area and diminish postoperative complications.

Challenges

Image analysis process

1. Skulls are movable and unstable when placed under the stereoscopic microscope. In order to diminish this error and make the process to be repeatable, skulls are placed on a plastic basement and fixed with plasticine clay in the Frankfurt horizontal plane.
2. To reduce measurement error, definition of each anatomical landmark is determined before the measurement and each parameter is measured twice.

Cadaveric dissection process

1. Soft tissue of some cadavers is frozen and hard which makes it difficult to palpate bony landmarks. In order to reduce this measurement error, we wait for the ice to melt for softer tissue, identify each point twice and use the average point for measurement
2. Pins might not fix properly when soft tissue is thin; therefore, we use color markers to mark where the pins are instead.

CHAPTER II
LITERATURE REVIEW

Infraorbital Foramen and Its Content

IOF is a foramen that lies on the maxilla bone and below infraorbital margin (1). It was found that there could be more than one foramen which is referred as AIOF. The existence of AIOF is varied in number, side and location (14, 16). Identifying the location of IOF is important because it contains neurovascular structures which are ION and IOA. The ION is branched from the maxillary nerve originating from infraorbital groove at the level of posterior maxillary wall, traveling along infraorbital canal and emerging from IOF (1). After exiting through the foramen, it gives off four branches; 1. Inferior palpebral branch which provides sensation to lower eyelids and conjunctivae. 2. Internal nasal branch which innervates some parts of nasal septum and vestibules of nose. 3. External nasal branch which distributes sensation to the lateral side of nose and 4. Superior labial branch which divides into lateral and medial subbranches and supplies sensation to upper lip and oral mucosa (2, 3) (Figure 1).

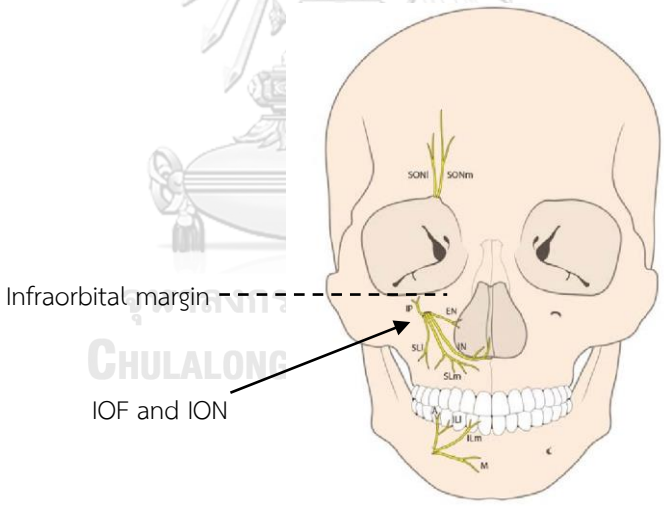

Figure 1. Drawing of a skull shows the location of IOF, ION and its distribution (17)
; Black dot line= the level of infraorbital margin, EN= external nasal nerve, IN= internal nasal nerve, IOF= infraorbital foramen, ION= infraorbital nerve, IP=inferior palpebral nerve, SLl= lateral branch of superior labial nerve, SLm= medial branch of superior labial nerve

The IOA commonly exits through IOF in the middle and superior (2) to the ION bundle within the same sheath (1). The ION could give off branches at various levels; at the beginning of infraorbital groove, along infraorbital canal or after emerging from IOF, and each branch can divide into subbranches differently (18). Hu et al. (2007) found that inferior palpebral branch of the ION divided into medial and lateral branches (3), while the study of Nderitu et al. (2014) reported only one branch of this nerve (19). Typically, the ION and its branches exit through IOF, but some fibers divide from the main nerve and emerge from other foramina separately. It was found that there were nerve and artery exiting through AIOF called AION and AIOA. From cadaveric dissection, nerve fibers emerging from AIOF can be any branches of the ION. Iwanaga et al. (2020) found that the AION had external nasal, inferior palpebral, internal nasal, and superior labial branches as same as the ION. The most common branch deriving from the AION was external nasal branch. Moreover, the study showed that both AION and AIOA originated from infraorbital canal and the AION and AIOA had communicating branches with the ION and IOA, respectively (Figure 2). From the result of this study, it was assumed that the AION could be a nerve bundle of the ION (15). The presence of the AION can explain why some patients experience impartial anesthesia after performing an adequate ION block (20, 21).

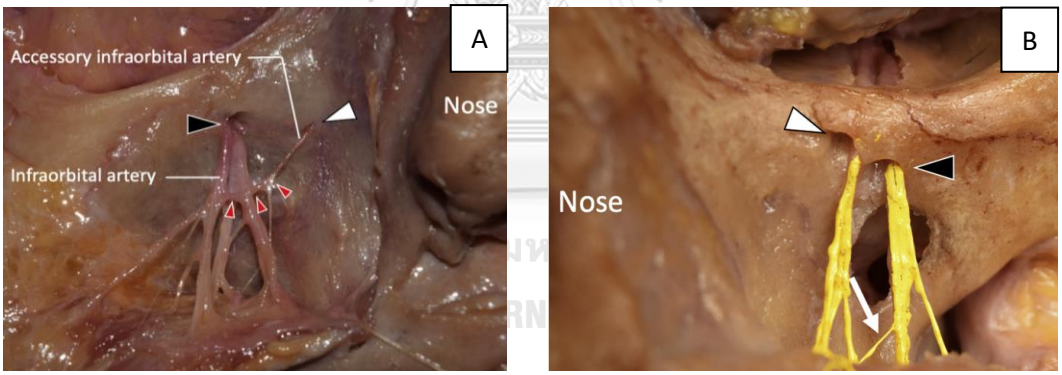

Figure 2. Cadaveric dissection shows association between neurovascular structures from IOF and AIOF. A. IOA anastomosing with AIOA B. ION and its communicating branches with AION *(15)*
; Black arrow head= infraorbital foramen, Red arrow head= communicating branches between IOA and AIOA, White arrow= communicating branches between ION and AION, White arrow head= accessory infraorbital foramen

Infraorbital Nerve Block

Peripheral nerve block is one of the regional anesthetic procedures that causes anesthesia of large specific area of the body innervated by the same nerve. The nerve block uses smaller amount of anesthetic drug than the local infiltration does and avoids tissue distortion (22, 23). The ION block is often used for achieving regional anesthesia of mid-facial

area. It provides numbness of the skin between lower eyelids, lateral side of nose, upper lip, upper premolars, upper incisors, lateral canines and gum (24). It can be performed by intraoral and extraoral approaches (22, 23). The intraoral approach seems to have a higher success rate and longer anesthetic effects (25).

The intraoral approach

Place the patient in seated position, have the patient looks straight ahead and draw an imaginary vertical line from mid-pupil to inferior border of infraorbital ridge. Place the finger over infraorbital margin, retract patient's cheek and insert the needle into oral mucosa 5 mm from the buccal surface above the first or second premolar. Insert the needle toward and in parallel with the teeth approximately 15 mm. Then draw the needle to check that it does not place into vessel and inject an anesthetic drug for 2–3 ml (22, 23, 26).

The extraoral approach

Place the patient in supine or seated position, have the patient looks straight ahead and draw an imaginary vertical line from mid-pupil to inferior border of infraorbital ridge. Place the finger 8–10 mm below infraorbital margin and palpate the foramen (12). Insert the needle through skin, subcutaneous tissue and muscle. Draw the needle to confirm that it does not place into vessel and inject an anesthetic solution until the surface tissue is swelling (22, 23, 26).

There might be complications following this procedure such as bleeding and hematoma due to direct pressure on an injection site, infections, unintentional injection into vessels, and nerve injury (26). Most of the complications are rare and reversible (24), however, there are also serious side effects. A sudden loss of vision due to central retinal arterial occlusion following the ION block was reported (27). The failure to achieve an anesthesia and its complications might be because of unusual anatomical structures and inappropriate blocking techniques.

Although the ION block is easy and safe to perform, the failure rate was high. There was a study about the success rate of performing percutaneous trigeminal nerve blocks. The results showed that the failure rate of trigeminal nerve blocks was 22% and the ION block performed by the extraoral approach had the highest failure rate which was 17% (13). Because IOF may not always be palpated, this can lead to failure of the procedure and complications. The success rate of this technique depends on experience of the physician in identifying the foramen and performing the procedure. This suggests that performing percutaneous nerve block requires basic knowledge of anatomical location of the foramen and nerve distributions.

The ION block technique is important in otorhinolaryngology, ophthalmology, maxillofacial surgery, plastic surgery and dentistry, for example, the polypectomy,

turbinectomy, septorhinoplasty (5, 6), repairing orbital floor fracture (7), surgical procedure involving soft tissue of the nose, cheek, lower eyelids and upper lip, and the cleft lip-cleft palate surgery (4). It is also considered to have benefit in reducing postoperative pain. Patients underwent the ION block following cleft lip repair and buccal mucosal graft urethroplasty had less postoperative pain score, required less analgesic drugs, and were able to eat earlier than those who had intravenous analgesics (28, 29). In an outpatient septorhinoplasty, the ION block can shorten time spent in post-anesthetic care unit, and reduce postoperative pain and tramadol requirement (5, 10). Bilateral ION block was also effectively used in controlling postoperative pain after the transsphenoidal hypophysectomy (11). Many studies found that neuropathic facial pain can be relieved by applying the ION block with neurolytic agents or performing a radiofrequency cautery to the ION (30, 31). Therefore, the ION block was considered a potential treatment option for treating an intractable infraorbital neuralgia in patient failing to resolve by standard medications (8, 9).

Location and Morphometric Study of Infraorbital Foramen

A number of studies tried to identify the location of IOF by using various landmarks in skulls and cadavers. Since the location of the foramen was described to be in the mid-pupillary line, the vertical distance from infraorbital margin was commonly measured. Even there was a consensus that IOF lies 8–10 mm below infraorbital margin (12), it was found that this distance ranged differently from 3.2–13.2 mm (32). The average distance between IOF and infraorbital margin was estimated to be 6-9 mm in skulls and cadavers (14, 32-41). Other reference points were also studied in skulls. The horizontal distance from facial midline to IOF ranged from 22.1–34.8 mm (32). The mean distance from piriform aperture to IOF varied from 14.72–17.23 mm in the horizontal direction (34, 35). The study in Brazilian skulls measured the mean distance from IOF to ANS which was 32.38 mm (34). While the study in Asian skulls found that this mean distance was 34.1 ± 0.2 mm on the right side and 33.3 ± 0.2 mm on the left side (38), in approximate to the study in African American and Caucasian population which was 34.1 mm and 33.05 mm, respectively (42). Moreover, the study in Asian skulls by Agthong et al. (2005) measured the angle between the horizontal line passing through ANS and IOF which had the mean value of 25.1 ± 0.4 degrees on the right side and 26.8 ± 0.4 degrees on the left side (38). The zygomaticomaxillary suture was another bony landmark used in localizing IOF. From the study in Indian population, the mean horizontal distance from IOF to the zygomaticomaxillary suture was 10.8 ± 2.7 mm and ranged from 3.8–16.8 mm (32). Whereas, this mean distance in African American population was 12.43 mm and in Caucasian population was 13.46 mm (42). Other examples of bony landmarks were nasion, lateral process of canine tooth (35), alveolar ridge of maxilla

at the second premolar (36), supraorbital foramen (32), nasolacrimal fossa and inferior orbital fissure (37). Table 1. shows the mean distance between IOF and bony landmarks that had been studied.

Soft tissue landmarks in cadavers were also determined as reference points. Kang-Jae Shin's study found that IOF located within 9 mm from the point where the vertical line passing through medial limbus crossed with the oblique line between lateral canthus and the peak of Cupid's bow (43) (Figure 3). Ercikti et al. (2017) found that IOF situated in the line between lateral canthus and ala nasi for 75% (40), while other studies suggested that IOF laid between medial limbus and mid-pupil (44) or within the mid-pupillary line (45). Kang-Jae Shin's study also found that the distance from IOF to facial midline was associated with vertical and horizontal dimensions of the midface (43). The mean horizontal distance from ala nasi to the vertical line through IOF was 4.9 mm with no statistically significant difference between sex and sides in the cadaveric study by Takahashi et al. (2011) (46). In other studies, this horizontal distance was 1.6 ± 2.7 mm and the distance between IOF and ala nasi was 15.9 ± 2.8 mm with the horizontal angle of 64.1° ± 9.9° between these structures (47). The distance between ala nasi and IOF in another study was 24.7 ± 4.0 mm which was largely different from previous studies (40). Lateral canthus was also determined as the reference point (48). The mean distance between IOF and lateral canthus was 30.5 ± 3.6 mm (40) and the vertical distance between them was 25.1 ± 2.0 mm (43). Other soft tissue landmarks such as angulus oculi medialis (49) and limbus (43) were also studied. Table 2. shows the distance between IOF and soft tissue landmarks.

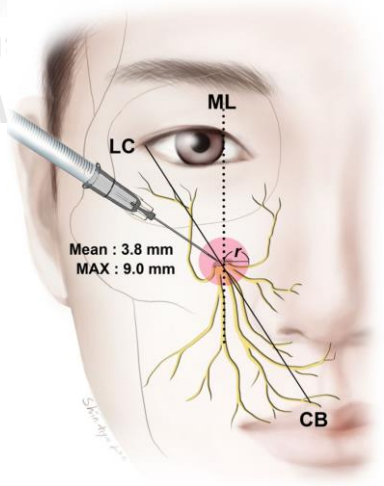

Figure 3. Picture shows IOF locating within 9 mm from the intersecting point between the oblique line from lateral canthus to the peak of Cupid's bow and the vertical line passing through medial limbus (43). ; CB= Cupid's bow, LC= lateral canthus, ML= medial limbus, r= radius

Previous studies showed that the location of IOF varied because size and anatomy of skulls depend on age, sex, race and reference points defined in each study. (35, 39, 50-56). In addition to the morphometric study in skulls and cadavers, the location of IOF was also analyzed in cone-beam computed tomography (CBCT) scan. The distance from IOF to infraorbital margin and facial midline were 7.98 ± 1.41 and 24.71 ± 2.09 mm which were similar to the study in skulls and cadavers. Another distance was the distance from IOF to lateral nasal wall (57) (Table 1).

The shape of IOF was different in each population. The study in adult Indian skulls found that the most common shape of IOF was oval (81.95%) and the second most common shape was circle (12.78%) (33), while the study in CBCT scan images of Lebanese population found that circle was the most common shape found (54.8%) and the second most common shape was oval (28.6%) (57). Size of the foramen also varied in each study. The width of IOF ranged from 1 to 7 mm (39). The mean width of the foramen was 3.23 mm (32) and 3.7mm (34, 57) in each study which had small difference. While the average transverse diameter of IOF in other studies were 2.72 mm (33) which was shorter and 5.5 mm (46) which was considerably longer than previous ones.

Location and Morphometric Study of Accessory Infraorbital Foramen

Many studies found multiple foramina as one of the variations of IOF. The systematic review conducted by Hwang et al. (2015) found that an overall frequency of skulls and cadavers having AIOF ranged from 0.8% to 27.3% (16). Later studies showed the difference in AIOF frequency. AIOF was found in 35% of skulls (57) and 36.7% in cadavers (15). The studies assessing CBCT scan images showed the prevalence of AIOF to be 29% (58), 56.6% (59) and 65.6% (14) which were extensively higher than previous studies. The prevalence of AIOF varied in each population. The prevalence of AIOF in Caucasian skulls was 21.7%, African American skulls was 10% (42), and Sri Lankan skulls was 7.4% (60) (Table 3).

The number of AIOF could range from 0 to 3 (16). The frequency of single and double foramen among AIOFs found in skulls were 85% and 14% (16, 61). Triple AIOF was also found in 1.25% of skulls (16). The study in CBCT scan found different number of AIOF. There was 94.33% of single AIOF, 4.96% of double AIOF and 0.71% of triple AIOF (59). Most of the AIOFs located unilaterally. The frequency of AIOF that occurred bilaterally ranged from 9.1% to 25% (14, 16, 58, 62). Many studies found that AIOF commonly located on the left side (14, 16, 38, 61, 63-65) of skulls, whereas some of the studies found it predominantly located on the right side (33, 66). Table 3 shows number and side of the AIOF found in each study.

Table 1. Distance from IOF to bony landmarks in skulls and CBCT scan images (Mean ± SD).

Specimen	Authors	Year	Infraorbital margin	Facial midline	Piriform aperture	Anterior nasal spine	Other landmarks
Dry skulls	Kazkayasi et al. (35)	2001	7.19 ± 1.39		17.23 ± 2.64		Nasion 43.46 ± 3.67 Canine tooth (lateral process) 33.94 ± 3.15
	Agthong, S., T. Huanmanop, and V. Chentanez (38)	2005	Rt. 7.8 ± 0.2 ® Lt. 8.0 ± 0.2 ®			Rt. 34.1 ± 0.2 ® Lt. 34.3 ± 0.2 ®	
	Gupta T. (32)	2008	7.0 ± 1.6	28.5 ± 2.6			Zygomaticomaxillary suture 10.8 ± 2.7 Supraorbital foramen 41.8 ± 3.7
	Rahman et al. (41)	2009		26		17	
	Chrcanovic, B.R., Abreu M.H.N.G., and Custódio A.L.N. (34)	2011	6.41 ± 1.69	25.26 ± 2.60	14.72 ± 2.02	32.38 ± 2.61	Zygomaticomaxillary suture 6.54 ± 1.68 Supraorbital foramen 42.92 ± 3.11
	Abed et al. (37)	2011	8.95 ± 1.53				Nasolacrimal fossa 20.67 ± 2.42 Inferior orbital fissure 25.40 ± 2.70
	Aggarwal et al. (33)	2015	6.33 ± 1.39	25.69 ± 2.37	15.19 ± 1.70		Maxillary alveolar border 28.41 ± 2.82
	Masabni O. and Ahmad M. (36)	2017	6.6 ± 1.65				Maxillary alveolar ridge at the second premolar 29.23 ± 1.65
	Polo et al. (14)	2018	6.55 ± 1.56		16.51 ± 1.91		Alveolar crest 30.34 ± 3.37
CBCT	Sokhn et al. (57)	2019	7.98 ± 1.41	24.71 ± 2.09	10.61 ± 2.39		

Unit: millimeters

® = mean and standard error of mean

Table 2. Distance from IOF to soft tissue landmarks in cadavers (Mean ± SD).

Specimen	Authors	Year	Infraorbital margin	Facial midline	Ala nasi	Lateral palpebral commissure	Angulus oculi medialis
Cadavers	Song et al. (47)	2007			15.9 ± 2.8		
	Takahashi, Y., H. Kakizaki, and T. Nakano (46)	2011			4.9		
	Zheng et al. (49)	2012			Superior 11.22 ± 2.01 Lateral 6.09 ± 2.32		Inferior 24.81 ± 3.39 Lateral 10.89 ± 2.78
	Ercikti, N., N. Apaydin, and Y. Kirici (40)	2017	8.8 ± 1.0	30.3 ± 2.7	24.7 ± 4.0	30.5 ± 3.6	
	Shin, K.J., H.J. Shin, and S.H. Lee (43)	2019		27.2 ± 2.2		25.1 ± 2.0	

Unit: millimeters

Table 3. Prevalence, number and side of AIOF

Specimen	Authors	Year	Prevalence	Number			Side		
				Single	Double	Triple	Right	Left	Bilateral
Dry skulls	Agthong et al. (38)	2005	4.09% (9/220 sides)	100% (9/9)			44.44% (4/9)	55.56% (5/9)	
	Gour et al. (63)	2010	4% (4/100 skulls)	75% (3/4)	25% (1/4)				
	Tezer et al. (65)	2011	7% (15/207 sides)				33.5% (5/15)	66.5% (10/15)	
	Rai et al. (66)	2013	13.6% (15/110 sides)				73.3% (11/15)	6.6% (1/15)	20% (3/15)
	Aggarwal et al. (33)	2015	21% (28/133 sides)		3.57% (1/28)				5.97% (4/67)
	Nanayakkara et al. (60)	2016	7.4% (4/54 skulls)						
	Nam et al. (61)	2017	35% (14/40 skulls)	30% (12/40)	5% (2/40)		42.86% (6/14)	57.14% (8/14)	
	Martin-Junior et al. (64)	2017	25.5% (48/188 sides)				47.92% (23/48)	52.08% (25/48)	
	Polo et al. (14)	2018	32.1% (27/84 sides, 30 AIOF)	88.89% (24/27)	11.11% (3/27)				16.7% (14/84)
	Zhang et al. (42)	2019	-Caucasian 21.7% (13/60) -African American 10% (6/60)						
Cadavers	Shin et al. (62)	2020	18.2% (8/44 sides)	87.5% (7/8)	12.5% (1/8)		62.5% (5/8)	37.5% (3/8)	25% (2/8)
	Iwanaga et al. (15)	2020	36.7% (11/30 heads)	100% (12/12)			66.67% (8/12)	33.33% (4/12)	9.09% (1/11)
Skulls & cadavers	Hwang et al. (16)	2014	0.8%–27.3%	85%	13.8%	1.25%	42.7%	45%	12%
CBCT	Dagistan et al. (59)	2016	56.4% (140/250 sides)	94.33% (133/140)	5% (7/140)	0.71% (1/140)			
	Ali et al. (58)	2017	29% (58/200 patients)	89.66% (52/58)	8.62% (5/58)	1.72% (1/58)	46.6% (27/58)	31% (18/58)	22.4% (13/58)

The majority of AIOFs situated superior and medial to IOF and the second most common site was inferomedial position (16, 64, 65). The mean distance from AIOF to IOF was 9.79 mm (9.60 ± 4.57 mm on the right side and 9.98 ± 2.67 mm on the left side) (66). Another study showed that the mean distance between AIOF and IOF was 3.95 ± 1.6 mm (65), while recent study in skulls found it to be 11.82 ± 4.59 mm (14). Table 4 describes the relationship between AIOF and IOF. The discordant results might be affected by studied population and measuring methods which were different and not thoroughly described in some studies. Other bony landmarks used as reference points for locating AIOF were frontomaxillary suture, zygomaticomaxillary suture and ANS (14, 64-66). In addition to skulls, the distance from AIOF to soft tissue landmarks were measured. In the cadaveric study, AIOF located 19.7 ± 1.7 mm vertically and 0.3 ± 3.5 mm horizontally from lacrimal caruncle. The horizontal distance of AIOF to facial midline was 22.2 ± 2.9 mm. This study also found that when drawing the vertical line through lacrimal caruncle crossing with the oblique line connecting lateral canthus with subnasal point, AIOF can be found within 8 mm from the intersecting point of these lines (62) (Figure 4). Table 5 shows the distance from AIOF to each landmark.

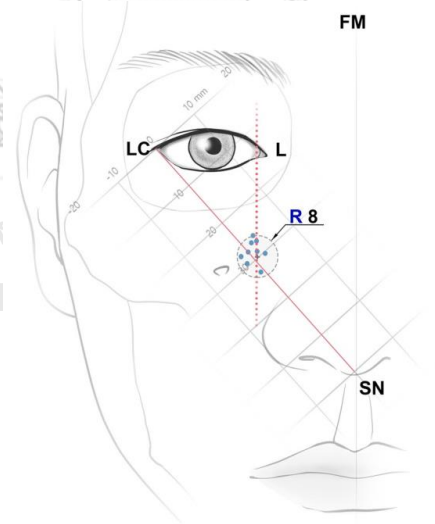

Figure 4. Picture shows AIOF locating within 8 mm from the intersecting point between the oblique line from lateral canthus to subnasal point and the vertical line passing through lacrimal caruncle (62).
; FM= facial midline, L= lacrimal caruncle, LC= lateral canthus, R= radius, SN= subnasal point

AIOF is defined as the foramen located near IOF. The study conducted by Zhang et al. (2019) considered that there might be two types of AIOF – the foramen located near IOF and the foramen within the sutura notha which is a vascular groove which lying lateral and

anterior to lacrimal crest and below infraorbital margin (Figure 5). Although this study reported that none of the AIOF along the sutura notha was connected to IOF (42), the study in CBCT scan images by Rusu et al. (2020) found that there was a connection between the foramen along the sutura notha and canaliculi from infraorbital canal. Moreover, the sutura notha might be an exit for some branches of ION and IOA (67). There were few studies that determined types of AIOF and it is still inconclusive whether foramina along the sutura notha are AIOFs.

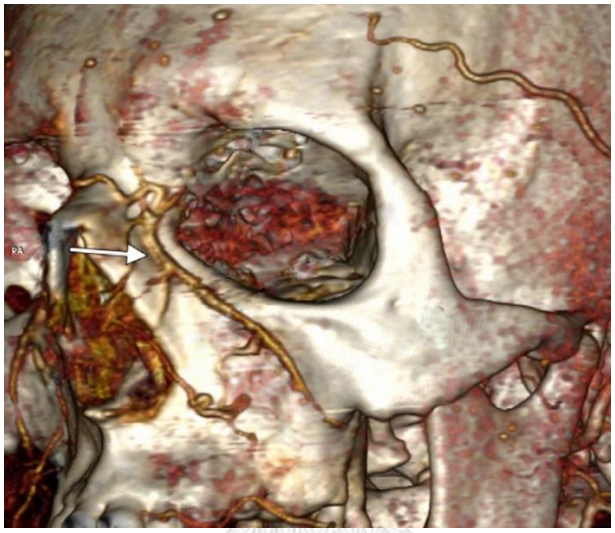

Figure 5. Three-dimensional reconstruction of skull shows the location of the sutura notha which is a vascular groove in front of the anterior lacrimal crest and below infraorbital margin (67).
; White arrow= the sutura notha

Table 4. Location and distance from AIOF to IOF (Mean ± SD).

Specimen	Authors	Year	Location of AIOF to IOF	Distance from AIOF to IOF
Dry skulls	Tezer et al. (65)	2011	Superomedial 93.3% (14/15) Inferomedial 6.7% (1/15)	3.95 ± 1.60
	Rai et al. (66)	2013	Superomedial 93.3 Medial 6.7%	Rt. 9.60 ± 4.57 Lt. 9.98 ± 2.67
	Aggarwal et al. (33)	2015	Superomedial 100%	
	Martin-Junior et al. (64)	2017	Superomedial 68.75% (33/48) Inferomedial 16.67% (8/48) Inferior 12.5% (6/48) Medial 2.08 (1/48)	Rt. 7.68 (1.29–16.76) ¶ Lt. 6.12 (2.54–13.32) ¶
	Polo et al. (14)	2018	Superomedial 86.7% (26/30) Medial 6.7% (2/30) Inferior 3.3% (1/30) Inferomedial 3.3% (1/30)	11.82 ± 4.59
	Zhang et al. (42)	2019	Proximal and connected with IOF 28.6% (4/14 skulls)	
Cadavers	Shin et al. (62)	2020	Superomedial 88.9% Medial 11.1%.	7.2 ± 2.4
	Iwanaga et al. (15)	2020	Medial 100% (12/12)	
Skulls and cadavers	Hwang et al. (16)	2014	Superomedial 92.2% (59/64) Inferomedial 7.8% (5/64)	
CBCT	Ali et al. (58)	2017	Superomedial 70.7% (41/58) Inferomedial 29.3% (17/58)	

Unit: millimeters

¶ median and interquartile range (IQR)

Table 5. Distance from AIOF to facial landmarks (Mean ± SD).

Specimen	Authors	Year	Infraorbital margin	Facial midline	Anterior nasal spine	Other landmarks
Dry skulls	Tezer et al. (65)	2011	5.61 ± 1.82	22.18 ± 2.56		Supraorbital foramen 39.92 ± 2.86 Nasomaxillary suture 21.95 ± 6.59
	Rai et al. (66)	2013	Rt. 4.51 ± 1.59 Lt. 4.86 ± 3.50		Rt. 25.14 ± 1.35 Lt. 26.46 ± 2.53	Frontomaxillary suture Rt. 25.63 ± 4.13 Lt. 22.32 ± 3.52 Zygomaticomaxillary suture Rt. 22.7 ± 5.49 Lt. 26.11 ± 5.64
	Martin-Junior et al. (64)	2017	Rt. 13.09 ± 6.33 Lt. 12.58 ± 4.83		Rt. 32.49 (30.25–36.75) ¶ Lt. 28.60 (26.62–32.23) ¶	Frontomaxillary suture Rt. 31.47 ± 9.88 Lt. 28.78 ± 7.00 Zygomaticomaxillary suture Rt. 22.48 ± 10.30 Lt. 24.88 ± 5.98
	Polo et al. (14)	2018	6.58 ± 3.09			Nasal aperture 10.93 ± 2.68
Cadavers	Shin et al. (62)	2020	6.4 ± 1.4	22.2 ± 2.9		Lacrimal caruncle - vertical 19.7 ± 1.9 - horizontal 0.3 ± 3.5
CBCT	Ali et al. (58)	2017	Rt. 10.3 ± 10.0 Lt. 10.3 ± 10.0			

Unit: millimeters,

¶ median and interquartile range (IQR)

CHAPTER III
MATERIALS AND METHODS

Sample Size Determination

1. From a pilot study of 10 skulls (20 sides), the standard deviation is of the vertical distance from the middle-upper edge of IOF to the line between ANS and Z (B) which is 2.82 mm. This study uses the sample size equation from the descriptive study and confidence interval is set at 95%

$$n = \frac{Z_{\alpha/2}{}^2\sigma^2}{d^2}$$

When $Z_{\alpha/2}{}^2 = Z_{0.05/2} = 1.96$ (two tail)

$\sigma^2 = (2.82)^2 = 7.93$

d = acceptable error = 0.5 mm

$$n = \frac{(1.96)^2(2.82)^2}{(0.5)^2} = 122.20$$

The calculated sample size of image analysis of skull is at least 123 sides of dry skulls. We include 432 sides from 216 skulls in this current study because we have a large number of dry skulls and the more sample we use, the more power of the study we can achieve.

2. From a pilot study of 5 cadavers (10 hemifaces), the standard deviation is of the shortest horizontal distance from the predicted IOF to the real IOF (F) which is 1.39 mm. This study uses the sample size equation from the descriptive study and confidence interval is set at 95%

$$n = \frac{Z_{\alpha/2}{}^2\sigma^2}{d^2}$$

When $Z_{\alpha/2}{}^2 = Z_{0.05/2} = 1.96$ (two tail)

$\sigma = (1.39)^2$

d = acceptable error = 0.5 mm

$$n = \frac{(1.96)^2(1.39)^2}{(0.5)^2} = 29.69$$

The calculated sample size of the cadaveric dissection process is at least 30 hemifaces of cadavers, so 30 hemifaces from 15 cadavers are included in this current study.

Equipment

1. Leica M50 Stereoscopic Microscope: Eyepieces lens 10x/23B with magnifier level 0.63x, Objective lens achromatic 0.32x with working distance 303 mm, Total Magnification 1.97x and Objective field diameter 116.8 mm

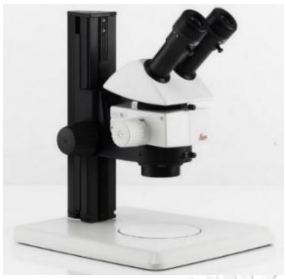

Objectives		Achr. 0.32×	
Working distance		303 mm	
Eyepiece	Mag. level	Total mag. ×	Obj. field ∅
10×/23B	0.63	1.97	116.8
	1.0	3.13	73.6
	1.6	5	46
	2.5	7.81	29.4
	4.0	12.5	18.4

Figure 6. Leica M50 Stereoscopic Microscope with 10x/23B eyepieces lens with magnifier level of 0.63x and objective lens with magnifier level of 0.32x (68).

2. Computer installed with Leica Application Suite (LAS) Core program V4.12
3. Plasticine clay
4. Plastic box
5. Stationaries i.e. calculator, pencils, color markers, rulers
6. Dissection instruments i.e. blade, forceps, scissors, probe, pins
7. Digital vernier caliper (Mitutoyo® 0-150 mm; range 150 mm, resolution 0.01 mm)

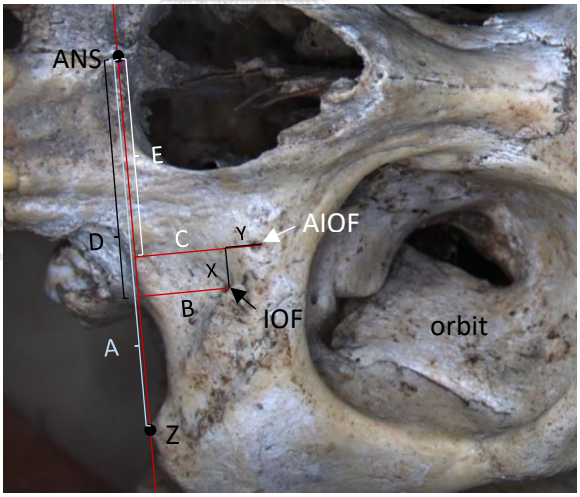

Figure 7. Picture of human dry skull describes parameters and measurement in this study.
; A= distance from ANS to the lowest point of the zygomaticomaxillary junction, AIOF= accessory infraorbital foramen, ANS= anterior nasal spine (tip of the intermaxillary suture of the maxilla bone), B= vertical distance from the middle-upper edge of IOF to line A, C= vertical distance from the middle-upper edge of AIOF to line A, D= distance from ANS to the intersecting point of the vertical line from IOF with line A, E= distance from ANS to the intersecting point of the vertical line from AIOF with line A, IOF= infraorbital foramen, X= horizontal distance between IOF and AIOF, Y= vertical distance between IOF and AIOF, Z= the lowest point of the zygomaticomaxillary junction

Research Framework

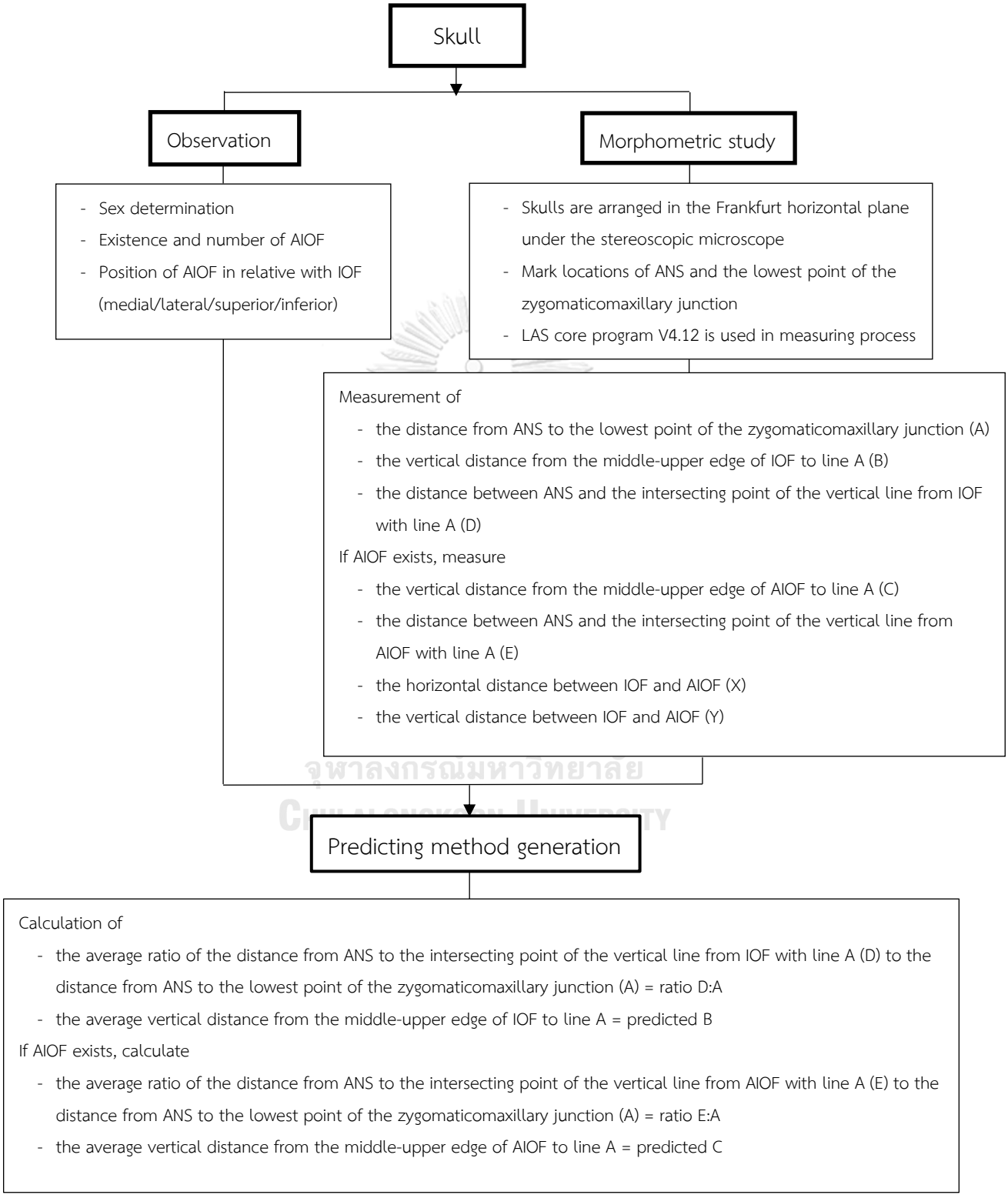

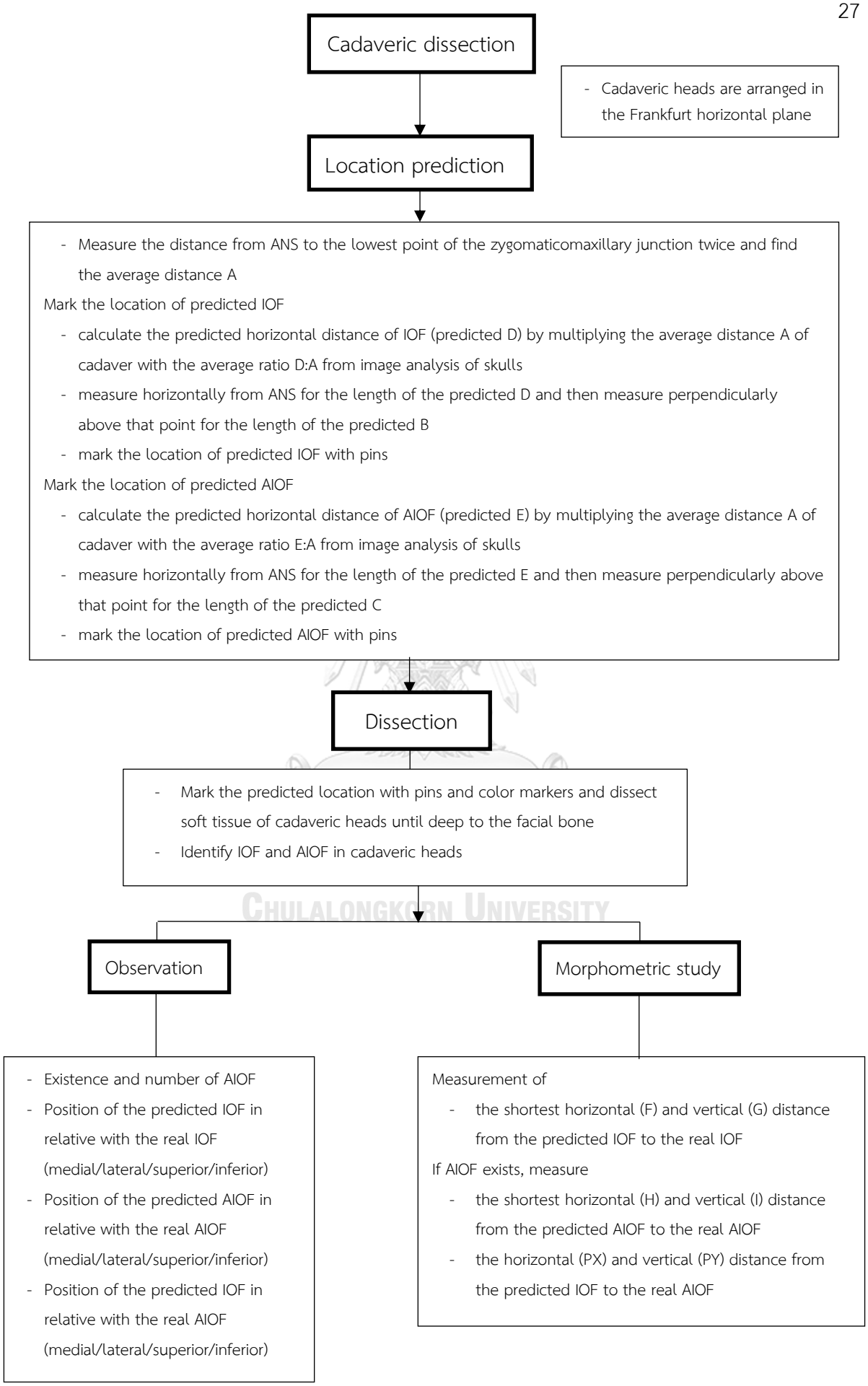

Methods

The process consists of two steps

1. Image analysis of skulls
2. Cadaveric dissection

I. Image Analysis of Skulls

1. Determine sex[1] of each skull by two observers separately. If there is any disagreement, the observers discuss to make a consensus.

[1] Nonmetric traits are used for determining sex of skulls because they can be assessed easily and quickly. There are many morphologic features for sex determination, for example, supraorbital ridges, glabella, orbits, nasal aperture, mastoid process, mental eminence, chin and tooth. According to the review of criteria for sex determination of skulls, general size and architecture should be used to establish the initial impression and supraorbital ridges are the second most common effective feature in sex determination (69). The most effective features are mandible and chin (69) which are not considered in this study because not all of the included skulls have mandible and chin. Mastoid process and occipital protuberance provide significant effective features of robusticity (69), so they are included in the criteria. General size and architecture, supraorbital ridges and mastoid process are also recommended features providing the high precision and accuracy for sex determination (70). Therefore, general size and architecture, supraorbital ridges, mastoid process and occipital protuberance are used for sex determination of skulls in this study (Figure 7). Table 6 shows four criteria used to distinguish between male and female skulls.

Table 6. Characteristics of male and female skulls

Criteria	Male	Female
General size and architecture	Large and rugged	Small and smooth
Supraorbital ridges	Prominent, thick and rounded	Less prominent and sharp
Mastoid process	Large volume	Small volume
Occipital protuberance	Large and marked muscular attachment	Small and not marked muscular attachment

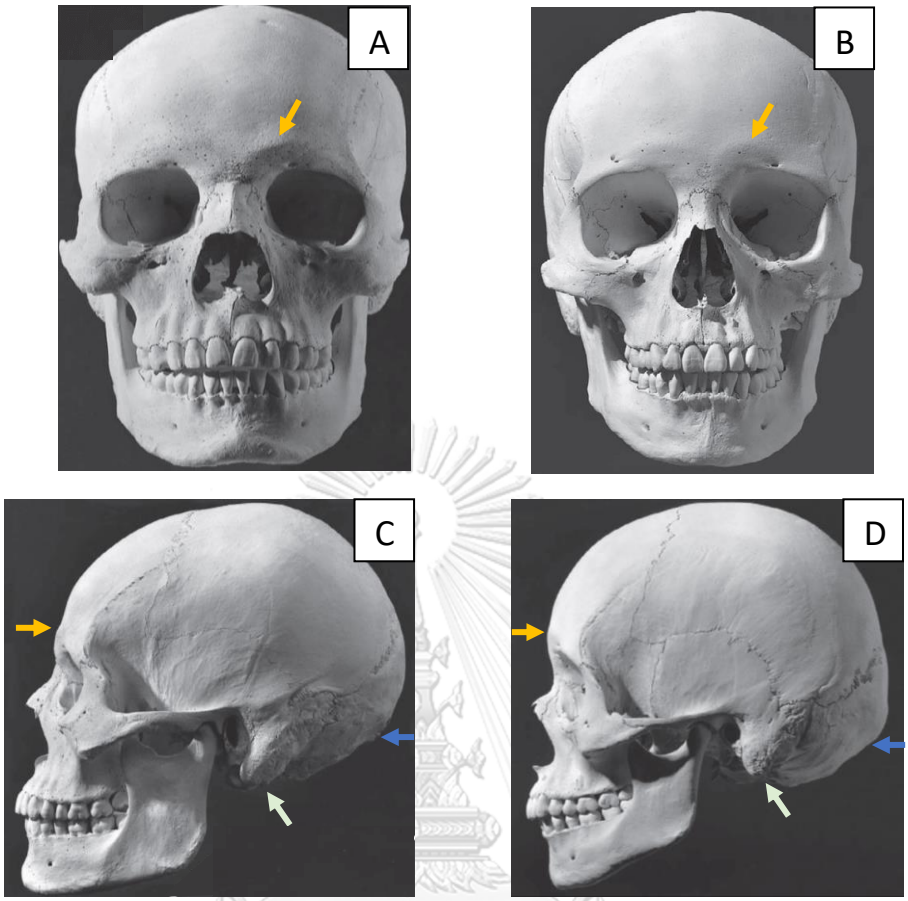

Figure 8. Pictures of male and female skulls show A. Male skull (anterior view) with prominent and thick supraorbital ridges B. Female skull (anterior view) with less prominent supraorbital ridges C. Male skull (lateral view) with prominent supraorbital ridges and occipital protuberance, and large volume of mastoid process D. Female skull (lateral view) with less prominent supraorbital ridges and occipital protuberance, and smaller volume of mastoid process (71) ; Blue arrow= occipital protuberance, White arrow= mastoid process, Yellow arrow= supraorbital ridge

2. Place the skull in supine position and arrange it in the Frankfort horizontal plane[2] under the stereoscopic microscope in anteroposterior view (Figure 8).

[2] Frankfort horizontal plane

There are many anatomical planes used for standardization in skull measurement (72, 73). The Frankfort horizontal or the German horizontal plane is considered the most approximate to the true horizontal plane when positioning in natural head position for craniometric study of skulls (72, 74-77). This plane is defined as the plane passing from the lowest point of infraorbital margin (orbitale) to the middle-upper

edge of auditory meatus (porion). It is widely used as the standardization for craniometric studies on skulls (78, 79).

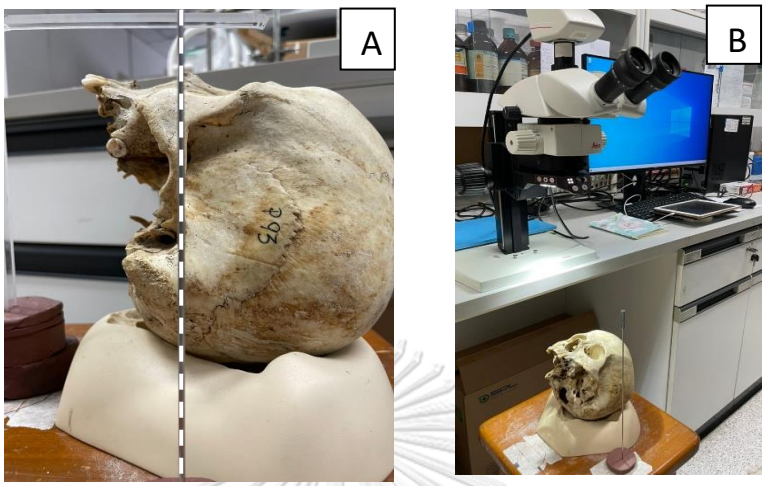

Figure 9. A. Skull in supine position arranged in the Frankfort horizontal plane. B. Picture shows the setting during the measuring process. Skull is placed under the stereoscopic microscope in anteroposterior view.; White dot line= the Frankfort horizontal plane

3. Mark the location of ANS and the lowest point of the zygomaticomaxillary junction with markers then place the skull under the Leica M50 Stereoscopic Microscope with achromatic lens 0.32x.

4. Use LAS core program V4.12 to capture live images and measure each distance. Check the setting of the stereoscopic microscope and the program every time before performing the measurement (Figure 9).

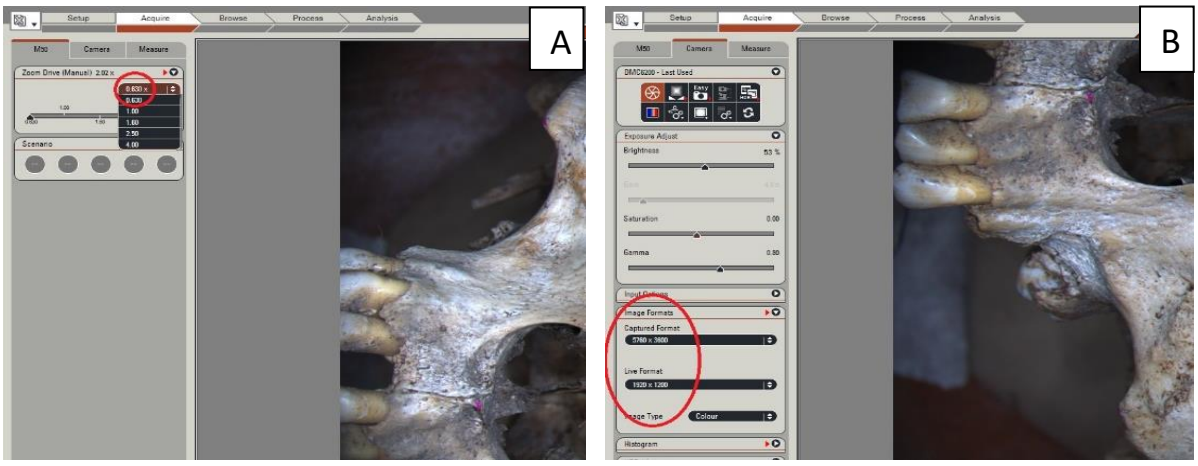

Figure 10. A. Set magnifier level of eyepieces to be 0.630X B. Set image format in the program to be 5760x3600 for captured format and 1920x1200 for live format.

5. Adjust camera exposure (white balance and color saturation) to get clear view of images (Figure 10).

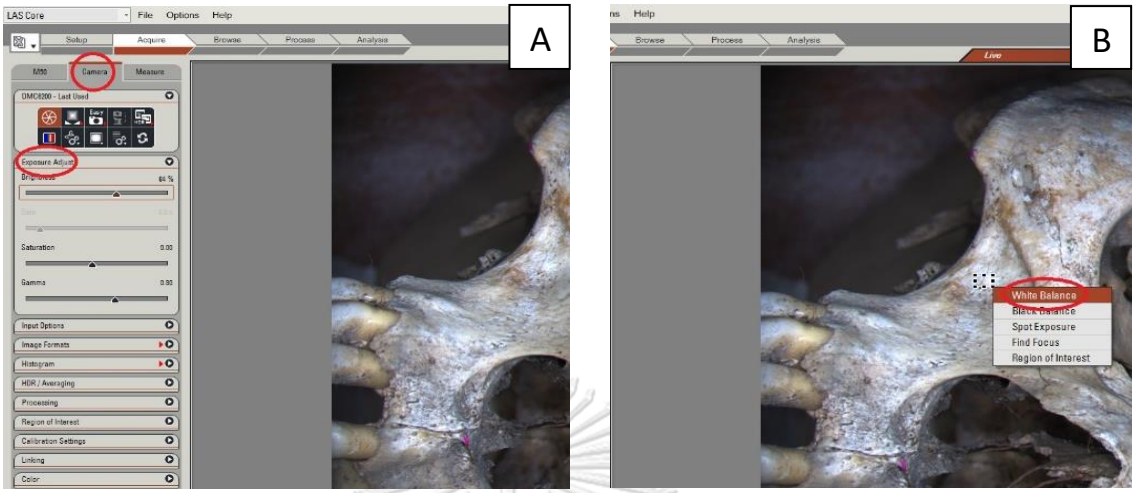

Figure 11. Adjust white balance and color saturation of images.

6. Use the Count Tool to mark the location of ANS which is at the tip of intermaxillary suture of the maxilla bone and the lowest point of the zygomaticomaxillary junction (Figure 11). Palpate bony landmarks under the camera to recheck with points marked in the previous step (Figure 12).

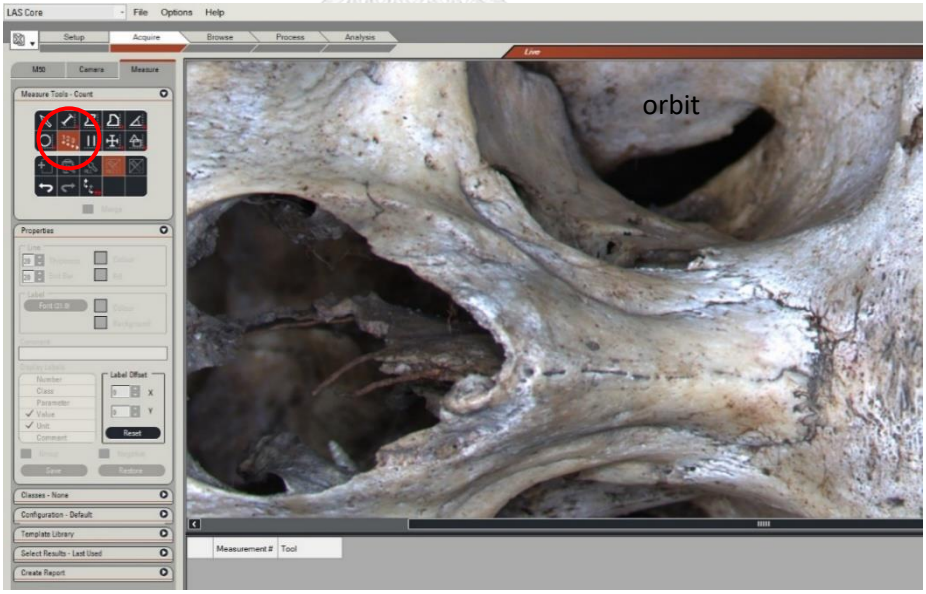

Figure 12. The Count Tool (red circle) used for marking bony landmarks in the LAS Core program

Figure 13. Palpate the bone to mark the location of ANS and recheck with the previously marked point. Live image is displayed in the program so we can palpate each point on the specimen during the measuring process.
; ANS= anterior nasal spine, White dot line= intermaxillary suture

7. Palpate the lowest point of the zygomaticomaxillary junction (Z) under the camera to recheck with the marked point and use the Distance Line Tool to measure the distance between ANS and Z (A) (Figure 13).

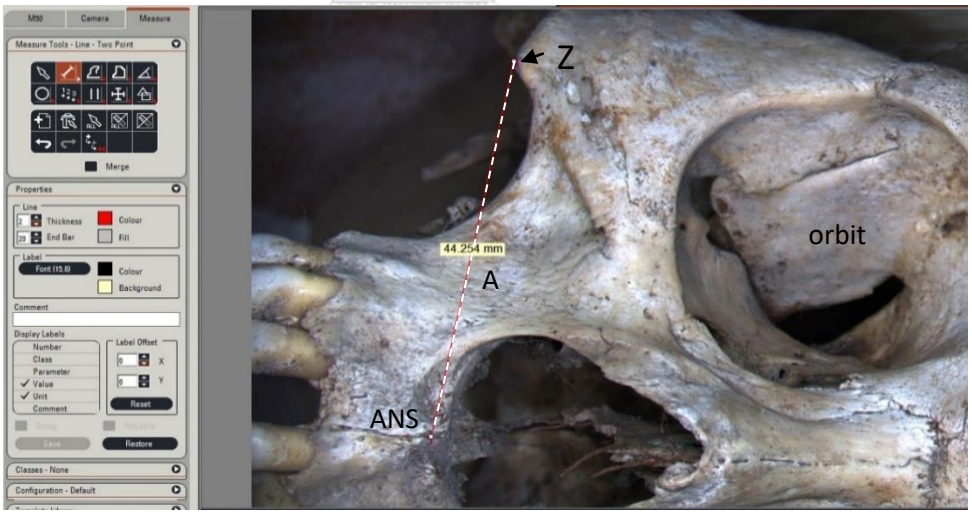

Figure 14. Measure the distance between ANS and the lowest point of the zygomaticomaxillary junction.
; White dot line (A)= line between ANS and the lowest point of the zygomaticomaxillary junction, ANS= anterior nasal spine, Z= the lowest point of the zygomaticomaxillary junction

8. Use the Parallel Line Tool to draw the horizontal line with line A and draw perpendicular lines from line A to the middle-upper edge of IOF (B) and AIOF (C) if it presents. Measure the distance B and C (Figure 14).

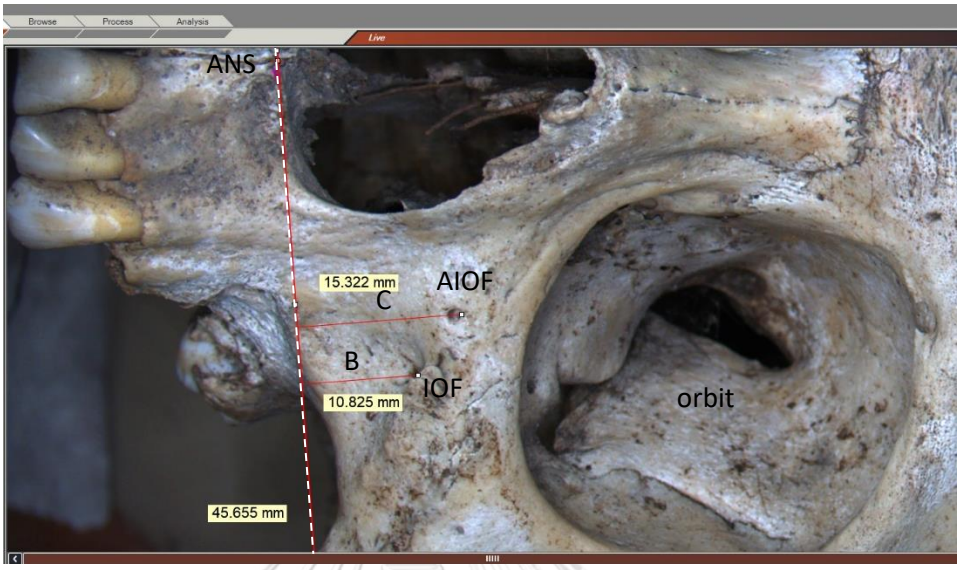

Figure 15. Draw the parallel and vertical lines to measure the distance from the middle-upper edge of IOF and AIOF to line A.
; White dot line= line A, AIOF= accessory infraorbital foramen, ANS= anterior nasal spine, B= vertical line from the middle-upper edge of IOF to line A, C= vertical line from the middle-upper edge of AIOF to line A, IOF= infraorbital foramen

9. Use the Distance Line Tool to measure the distance from ANS to the intersecting point of the vertical line from IOF with line A (D) and to the intersecting point of the vertical line from AIOF with line A (E) if AIOF exists (Figure 15).

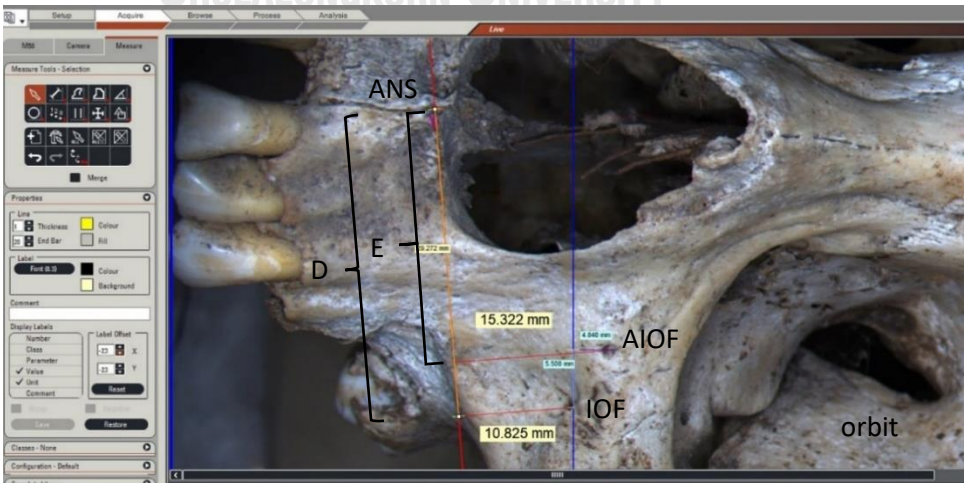

Figure 16. Measure the distance from ANS to the intersecting point of the vertical line from IOF and AIOF with line A.

; Blue line= the line in parallel with the vertical border of the picture, AIOF= accessory infraorbital foramen, ANS= anterior nasal spine, D= distance from ANS to the intersecting point of the vertical line from IOF with line A, E= distance from ANS to the intersecting point of the vertical line from AIOF with line A, IOF= infraorbital foramen

10. If AIOF exists, an additional parallel line is drawn. Use the Multiple Distance Line Tool to draw the line parallel with the vertical border of the image that passes through the middle-upper edge of IOF and use the Parallel Distance Line to draw the vertical line from the middle-upper edge of AIOF to this new parallel line to measure the vertical distance between IOF and AIOF (Y) (Figure 16).

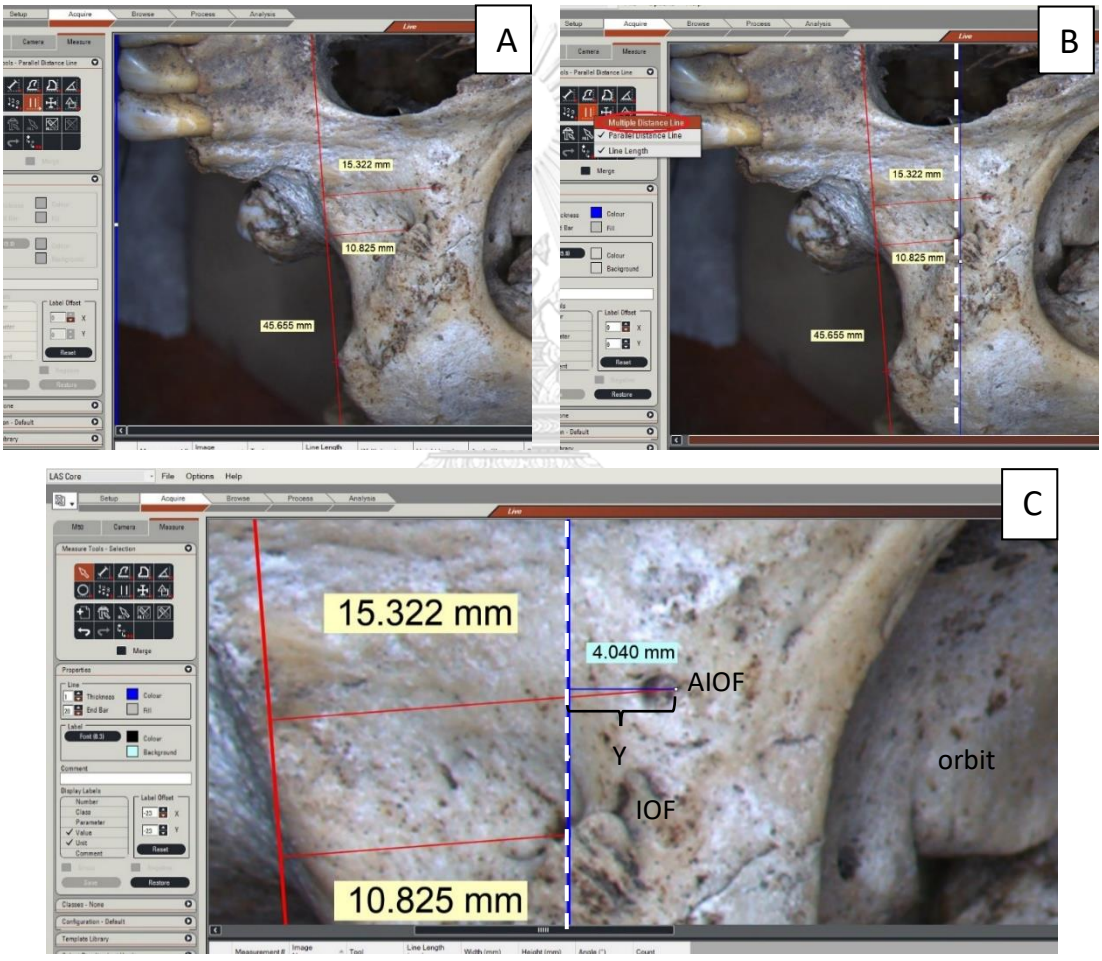

Figure 17. A. Blue line parallel with the vertical border of the image B. Draw a new parallel line by using the Multiple Distance Line Tool (red circle) C. Measure the vertical distance between IOF and AIOF.

; Blue line= the line in parallel with the vertical border of the picture, White dot line= parallel line passing through the level of the middle-upper edge of IOF, AIOF= accessory infraorbital foramen, IOF= infraorbital foramen, Y= vertical distance between IOF and AIOF

11. Use the Distance Line Tool to measure the distance from IOF to the intersecting point of the vertical line from AIOF with the new parallel line (X) (Figure 17).

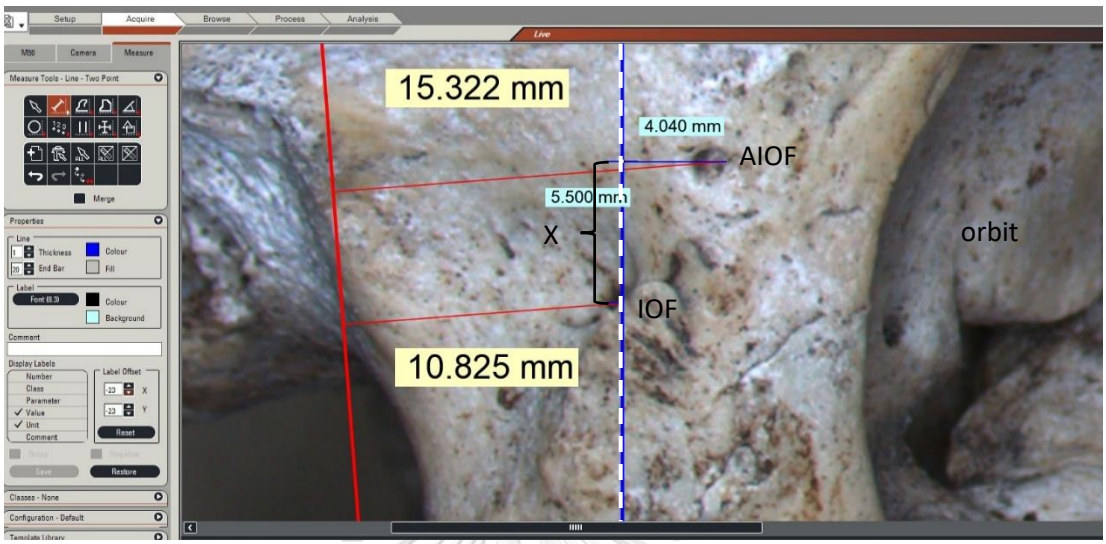

Figure 18. Measure the horizontal distance between IOF and AIOF.
; White dot line= parallel line passing through the level of the middle-upper edge of IOF, AIOF= accessory infraorbital foramen, IOF= infraorbital foramen, X= horizontal distance between IOF and AIOF

12. Repeat step 2 to 11 in another side of the same skull. All parameters are measured twice.

II. Cadaveric Dissection

1. The cadaveric head is arranged in the Frankfurt horizontal plane (Figure 18).

Figure 19. Cadaver is arranged in the Frankfort horizontal plane.
; White dot line= the Frankfort horizontal plane

2. ANS and the lowest point of the zygomaticomaxillary junction are marked with pins. Then, draw the horizontal line between these two points (line A). The surface location of ANS is defined as the uppermost part of philtrum at the level of nostrils and Z is the lowest bony prominence of cheek (Figure 19).

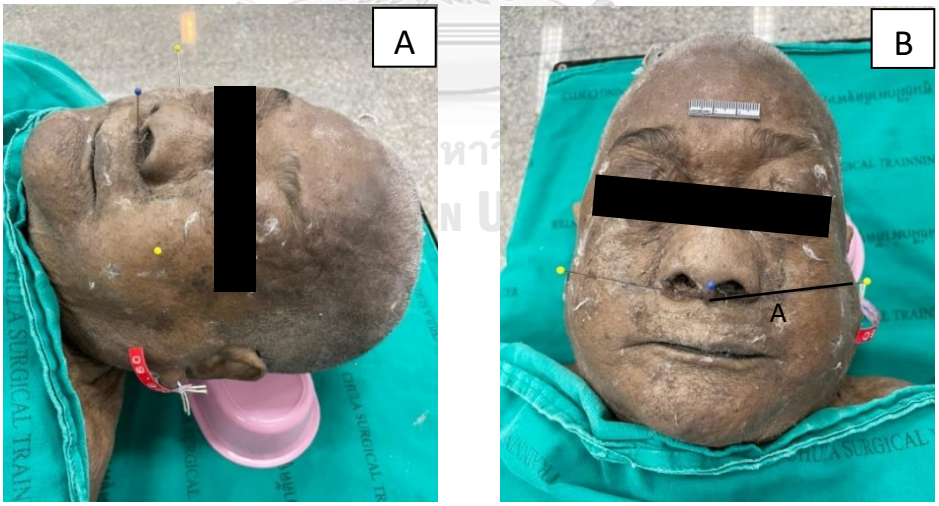

Figure 20. A. ANS and the lowest point of the zygomaticomaxillary junction are marked with pins. B. Draw the horizontal line between ANS and the lowest point of the zygomaticomaxillary junction.
; Blue pin= location of anterior nasal spine, Yellow pin= location of the lowest point of the zygomaticomaxillary junction, A= line from ANS to the lowest point of the zygomaticomaxillary junction

3. Measure the distance of line A twice and find the average distance A. Calculate the predicted horizontal distance of IOF (Predicted D) by multiplying the average distance A of the cadaver with the average ratio of D:A. Calculate the predicted horizontal distance of AIOF (Predicted E) by multiplying the average distance A of the cadaver with the average ratio of E:A. Mark each point with pins (Figure 20).

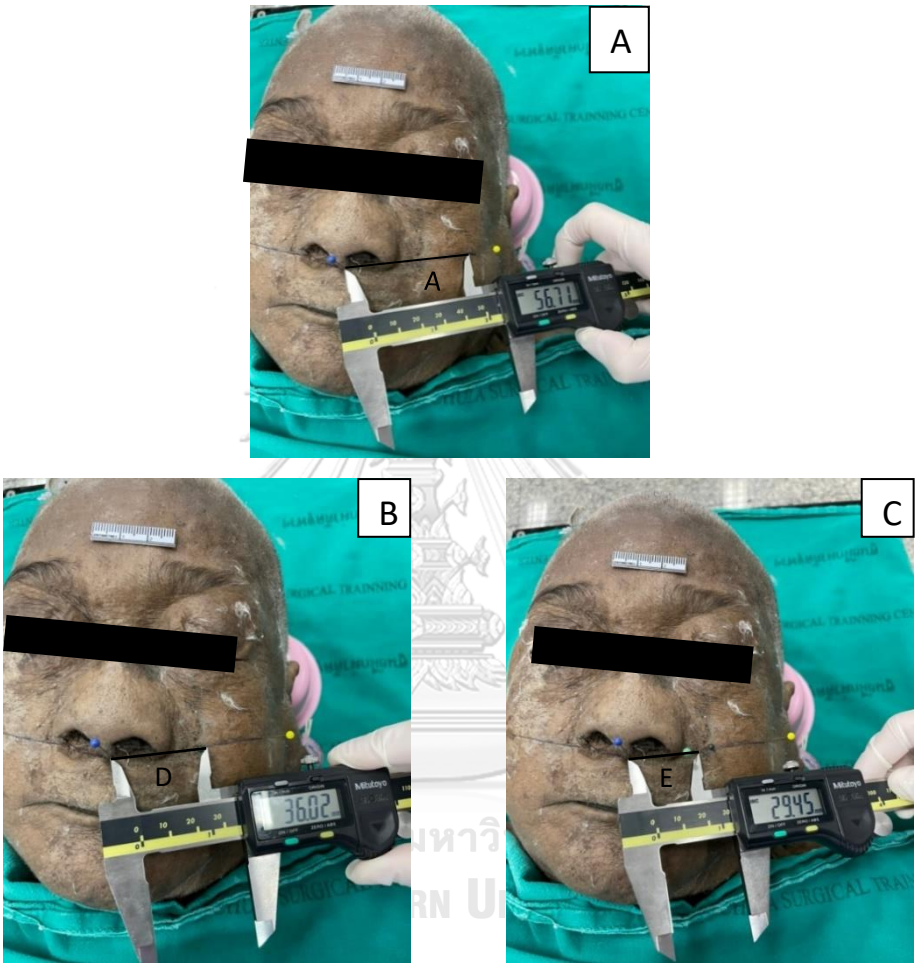

Figure 21. A. Measure the distance between ANS and the lowest point of the zygomaticomaxillary junction twice and find the average distance A B. Mark the predicted horizontal distance of IOF from ANS. C. Mark the predicted horizontal distance of AIOF from ANS.
; Blue pin= location of anterior nasal spine, Yellow pin= location of the lowest point of the zygomaticomaxillary junction, A= line from ANS to the lowest point of the zygomaticomaxillary junction, D= predicted horizontal distance of IOF, E= predicted horizontal distance of AIOF

4. Measure perpendicularly with line A from the predicted horizontal location of IOF (predicted D) for the length of the predicted B to get the predicted location of IOF and mark this point with pin. Also, measure perpendicularly with line A from the

predicted horizontal location of AIOF (predicted E) for the length of the predicted C to get the predicted location of AIOF and mark this point with pin (Figure 21).

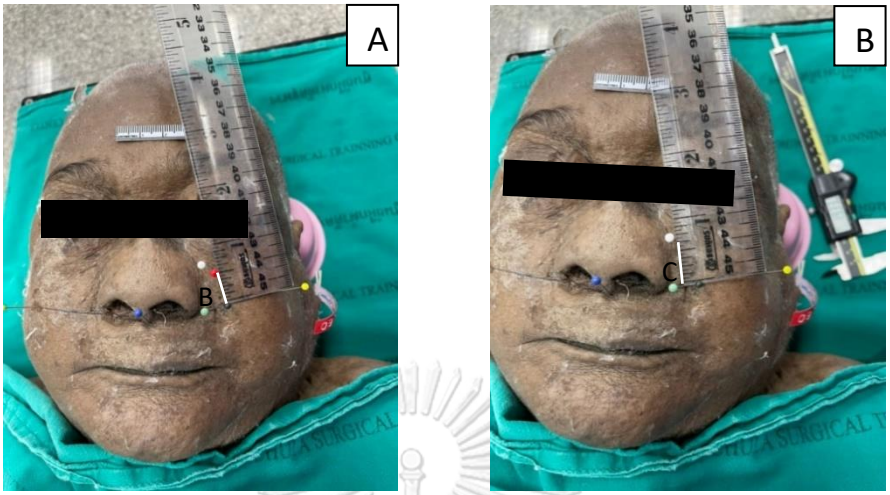

Figure 22. A. Measure perpendicularly with line A from the predicted horizontal location of IOF for the length of the predicted B and mark this point with pin. B. Measure perpendicularly with line A from the predicted horizontal location of AIOF for the length of the predicted C and mark this point with pin.
; Blue pin= location of anterior nasal spine, Dark green pin= the predicted horizontal location of IOF, Light green pin= the predicted horizontal location of AIOF, Red pin= location of the predicted IOF, White pin= location of the predicted AIOF, Yellow pin= location of the lowest point of the zygomaticomaxillary junction, B= predicted vertical distance from IOF to line A, C= predicted vertical distance from AIOF to line A

5. Dissect soft tissue deep to bone to identify the real IOF and AIOF. If pins couldn't be fixed on soft tissue, color markers are used instead (Figure 22).

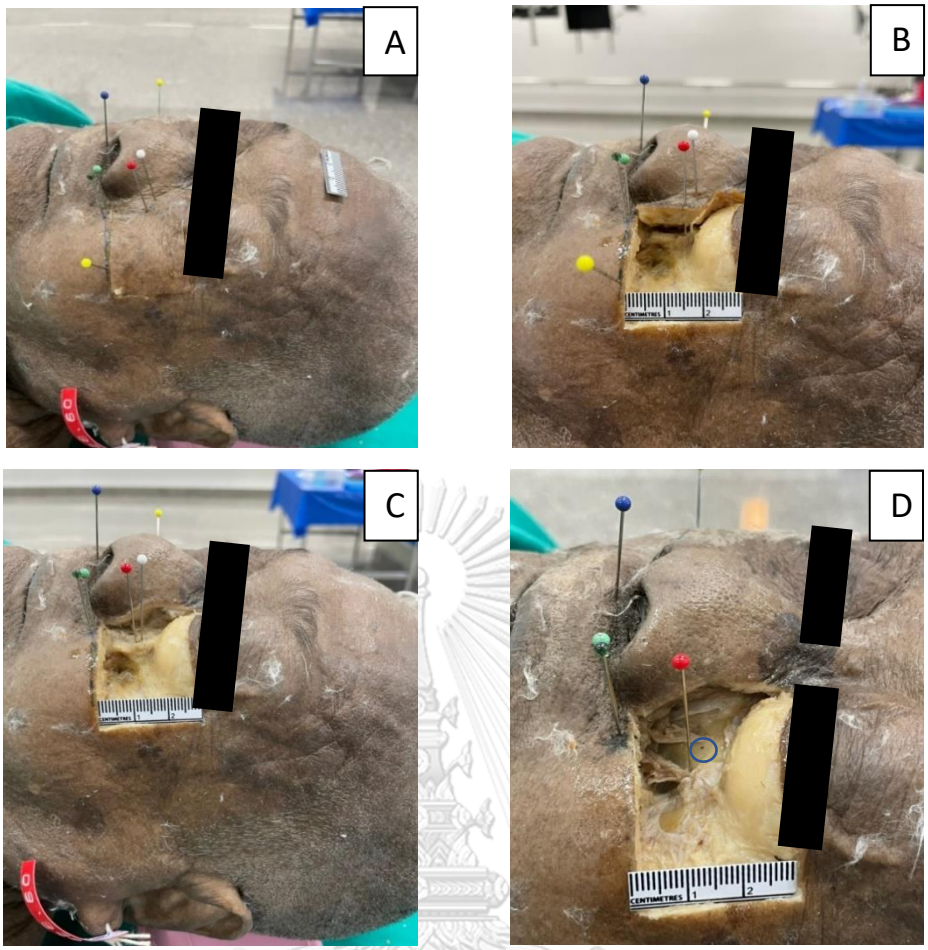

Figure 23. Dissect in the order from picture A → B → C → D to identify the real IOF and AIOF. ; Blue dot in the blue circle= location of the predicted AIOF, Blue pin= location of anterior nasal spine, Red pin= location of the predicted IOF, White pin= location of the predicted AIOF, Yellow pin= location of the lowest point of the zygomaticomaxillary junction

6. Measure the distance from the predicted IOF to the real IOF in horizontal (F) and vertical (G) directions. If AIOF exists, measure the distance from the predicted AIOF to the real AIOF in horizontal (H) and vertical (I) directions. Also, measure the horizontal (PX) and vertical (PY) distance from the predicted IOF to the real AIOF (Figure 23).

Lateral view Superior view

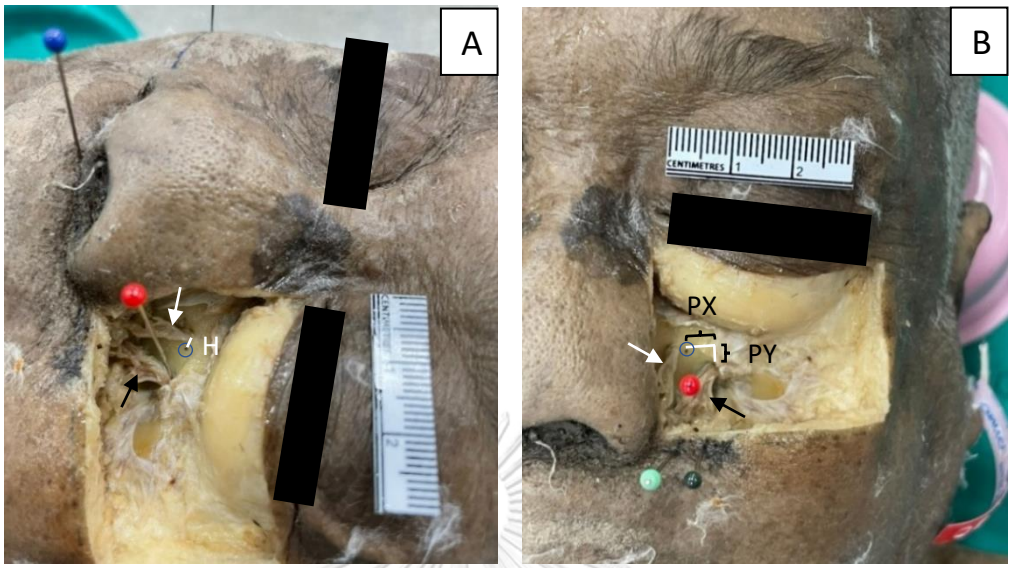

Figure 24. A. Measure the shortest horizontal distance from the predicted AIOF to the real AIOF. B. Measure the horizontal and vertical distance from the predicted IOF to the real AIOF.
; Black arrow= ION emerging from IOF, Blue dot in blue circle= location of the predicted AIOF, Blue pin= location of anterior nasal spine, Dark green pin= the predicted horizontal location of IOF, Light green pin= the predicted horizontal location of AIOF, Red pin= location of the predicted IOF, White arrow= AION emerging from AIOF, H= the shortest horizontal distance from the predicted AIOF to the real AIOF, PX= the horizontal distance from the predicted IOF to the real AIOF, PY= the vertical distance from the predicted IOF to the real AIOF

7. Repeat the step 1 to 6 in another side of the same cadaveric head. All parameters are measured twice.

CHAPTER IV
RESULTS

Prevalence, Number and Location of AIOF

This study included 432 sides from 216 skulls. There were 63 female skulls with 126 sides and 153 male skulls with 306 sides. The prevalence of AIOF was 19.91% (86 AIOFs from 432 sides) which located on the left side for 46 foramens (53.49%) and on the right side for 40 foramens (46.51%). A single AIOF was found in 82 sides of skulls. Double AIOFs were found in two male skulls presented on the left (Figure 24) and right side. No triple AIOF was observed in this study. There were 21 from 42 skulls (50%) of which AIOF presented bilaterally. Regarding to sex, the prevalence of AIOF is 19.61% (60 AIOFs from 306 sides) and 20.63% (26 AIOFs from 126 sides) in male and female skulls respectively. Detailed information of AIOF in this study is shown in Table 7. Most of the AIOFs located superomedial to IOF (Figure 25) except for 3 AIOFs which located in the inferolateral position (Figure 26). AIOF located 6.10 ± 2.20 mm medial (X) and 4.10 ± 2.06 mm superior (Y) to IOF (Figure 27).

Table 7. Number of AIOF according to sex, side and location in relative with IOF

	Total	Sex		Side	
		female	male	Left	Right
Sides of skulls	432	126	306	432	432
Number of AIOF (n)	86	26	60	46	40
Single AIOF (n)	82	26	56	44	38
Double AIOF (n)	4	0	4	2	2
Superomedial to IOF (n)	83	25	58	44	39
Inferolateral to IOF (n)	3	1	2	1	2

AIOF= accessory infraorbital foramen, IOF= infraorbital foramen, n= number

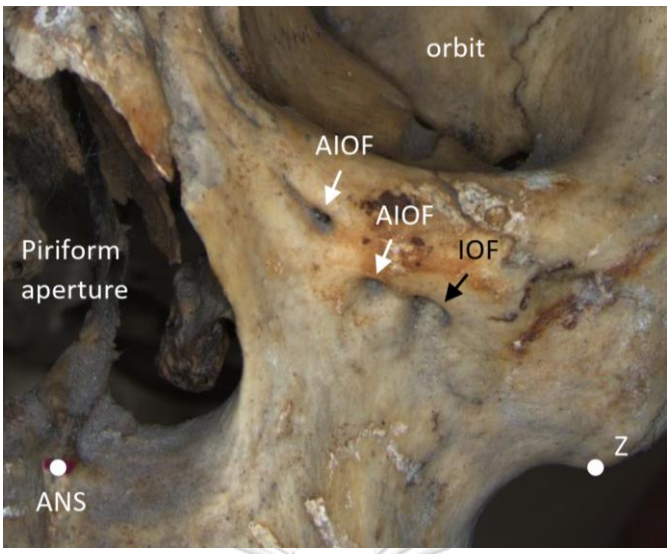

Figure 25. Picture of the left sided skull (number 66-073) shows double AIOFs.
; AIOF= accessory infraorbital foramen, ANS= anterior nasal spine, IOF= infraorbital foramen, Z= the lowest point of the zygomaticomaxillary junction

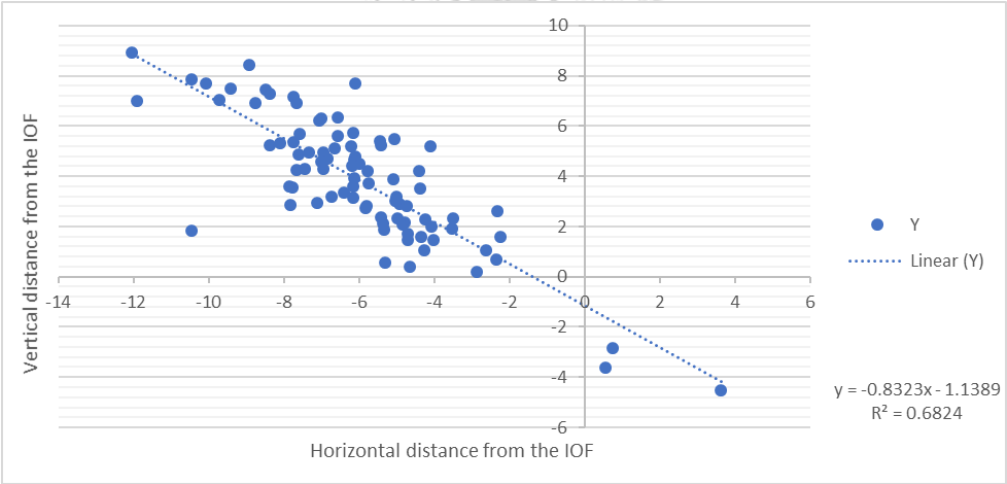

Figure 26. Scatter plotted graph shows the location of AIOF (blue dot) with reference to IOF (the origin or (0,0) point).
; X= horizontal distance between IOF and AIOF, Y= vertical distance between IOF and AIOF

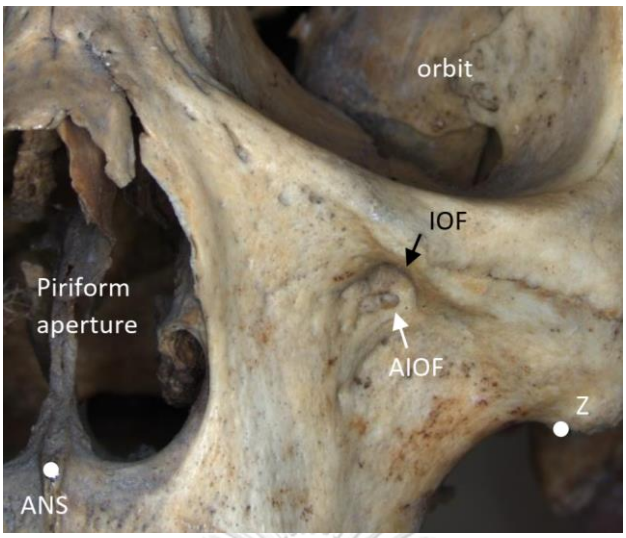

Figure 27. Picture of the left sided skull (number 1-195) shows AIOF in the inferolateral position to IOF.
; AIOF= accessory infraorbital foramen, ANS= anterior nasal spine, IOF= infraorbital foramen, Z= the lowest point of the zygomaticomaxillary junction

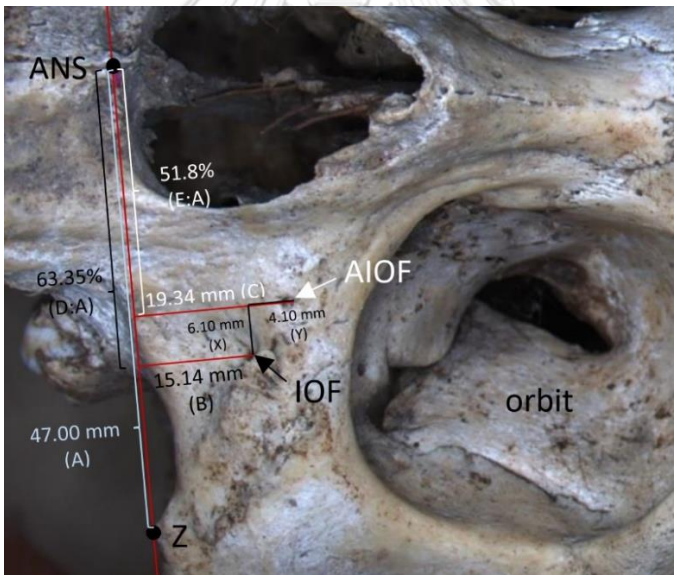

Figure 28. Picture of skull illustrates the mean value of main parameters of IOF and AIOF with reference to the line from ANS to the lowest point of the zygomaticomaxillary junction.
; A= distance from ANS to Z, AIOF= accessory infraorbital foramen, ANS= anterior nasal spine, B= vertical distance from the middle-upper edge of IOF to line A, C= vertical distance from the middle-upper edge of AIOF to line A, D= horizontal distance from ANS to the intersecting point of the vertical line from IOF with line A, D:A= percentage of the ratio of distance D to distance A, E= horizontal distance from ANS to the intersecting point of the vertical line from AIOF with line A, E:A= percentage of the ratio of distance E to distance A, IOF= infraorbital foramen, X= horizontal distance between IOF and AIOF, Y= vertical distance between IOF and AIOF, Z= the lowest point of the zygomaticomaxillary junction
Unit: millimeters

Predicting Method for Localization of IOF and AIOF

The line from ANS to the lowest point of the zygomaticomaxillary junction (A) was the main reference plane in this study. The mean distance of line A was 47.00 ± 2.95 mm. The mean distance from ANS to the intersecting point of the vertical line from IOF with line A (D) was 29.75 ± 2.32 mm. The mean distance from ANS to the intersecting point of the vertical line from AIOF with line A (E) was 24.41 ± 3.11 mm. The mean ratio D:A was 63.35 ± 3.90% and the mean ratio E:A was 51.80 ± 5.90%. The vertical distance from the middle-upper edge of IOF (B) and AIOF (C) to line A were 15.14 ± 1.99 mm and 19.34 ± 3.36 mm, respectively (Figure 27). There were statistically significant differences between sex in the distance A and distance D ($p<0.05$), other parameters had no statistically significant difference between sex and sides (Table 8). The mean ratio of distance D to A and the mean distance B were used to predict the location of IOF, whereas, the mean ratio of distance E to A and the mean distance C were used as the predicting method for localization of AIOF. The values of each studied parameter are listed in Table 8.

Table 8. Distance A, B, C, D, E, X and Y from image analysis of skulls (Mean ± SD).

Parameter (mm)	Side			Sex			Total
	Left	Right	p value	Male	Female	p value	
A	47.04 ± 2.96	46.97 ± 2.94	0.711	47.46 ± 2.90	45.90 ± 2.78	<0.001*	47.00 ± 2.95
B	15.12 ± 2.03	15.16 ± 1.95	0.711	15.18 ± 1.94	15.05 ± 2.11	0.533	15.14 ± 1.99
C	19.42 ± 3.20	19.25 ± 3.57	0.200	19.50 ± 3.13	18.98 ± 3.87	0.510	19.34 ± 3.36
D	29.81 ± 2.35	29.69 ± 2.29	0.481	30.06 ± 2.25	29.00 ± 2.32	<0.001*	29.75 ± 2.32
E	24.62 ± 2.66	24.16 ± 3.59	0.483	24.60 ± 3.26	23.95 ± 2.73	0.374	24.41 ± 3.11
X	5.91 ± 2.04	6.32 ± 2.38	0.837	6.22 ± 2.38	5.83 ± 1.72	0.453	6.10 ± 2.20
Y	4.00 ± 2.13	4.22 ± 2.01	0.214	4.08 ± 2.24	4.16 ± 1.62	0.845	4.10 ± 2.06
D:A (%)	63.42 ± 4.02	63.26 ± 3.79	0.725	63.40 ± 4.00	63.21 ± 3.66	0.662	63.35 ± 3.90
E:A (%)	52.40 ± 5.27	51.11 ± 6.56	0.753	51.54 ± 6.35	52.41 ± 4.77	0.534	51.8 ± 5.90

A= distance from ANS to the lowest point of the zygomaticomaxillary junction, B= vertical distance from the middle-upper edge of IOF to line A, C= vertical distance from the middle-upper edge of AIOF to line A, D= horizontal distance from ANS to the intersecting point of the vertical line from IOF with line A, E= horizontal distance from ANS to the intersecting point of the vertical line from AIOF with line A, X= horizontal distance between IOF and AIOF, Y= vertical distance between IOF and AIOF, D:A= percentage of the ratio of distance D to distance A, E:A= percentage of the ratio of distance E to distance A

Unit: millimeters

* statistically significant difference between groups

Accuracy Assessment of the Predicting Method in Cadavers

Dissection and measurement were performed in 15 cadavers (8 male and 7 female). From 30 IOFs in cadavers, the predicted IOF was found accurately in the same position with the real IOF for 15 sides (50%) (Figure 28). There were 10 (33.33%), 3 (10%) and 2 (6.67%) of the predicted IOF that located lateral (Figure 29), inferior and inferolateral to the real IOF, respectively. The mean error distance of the predicted IOF was 1.10 ± 1.44 mm lateral (F) to and 0.59 ± 1.39 mm inferior (G) to the real IOF (Figure 30).

Figure 29. Picture of the left midface of male cadaver (number B20860) shows the same location of both the predicted IOF and the real IOF (tip of red pin). The predicted AIOF locates lateral to the real AIOF. ; AIOF= accessory infraorbital foramen, ANS= anterior nasal spine, IOF= infraorbital foramen, ION= infraorbital nerve, Z= the lowest point of the zygomaticomaxillary junction, Black line= the line between ANS and the lowest point of the zygomaticomaxillary junction, Blue dot= location of the predicted AIOF, Blue pin= location of anterior nasal spine, Dark green pin= location of the predicted distance D (average distance A of the cadaver multiplied with the average D:A), Light green pin= location of the predicted distance E (average distance A of the cadaver multiplied with the average E:A), Red pin= location of the predicted IOF

There were only two single AIOFs identified on the left side of male and female cadaver and there was no double or triple AIOF. The prevalence of AIOF was 6.67% (2 AIOFs from 30 sides). All predicted AIOFs located lateral to real AIOFs and the mean horizontal distance error (H) was 1.83 ± 0.15 mm. No vertical distance error (I) was detected. The real AIOFs were all located superomedial to the predicted IOFs. The mean distance from the predicted IOF to the real AIOF was 5.56 ± 0.81 mm (PX) and 6.56 ± 0.68 mm (PY) in horizontal and vertical directions. Figure 30 represents the mean distance error between the

predicted and real foramen in cadavers (the picture used for illustration is the picture of skull for easier understanding). There was statistically significant difference in the mean horizontal distance from the predicted IOF to the real IOF between sides ($p<0.05$), other parameters had no statistically significant difference between sex and sides. The values of each parameter are shown in Table 9.

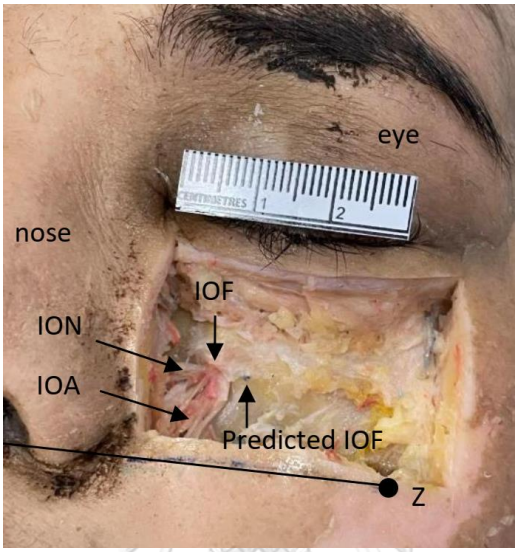

Figure 30. Picture of the left midface of female cadaver (number 61B069F) shows the predicted IOF locating lateral to the real IOF. This midface had no AIOF.
; Black line= line between ANS and the lowest point of the zygomaticomaxillary junction, IOA= infraorbital artery, IOF= infraorbital foramen, ION= infraorbital nerve, Z= the lowest point of the zygomaticomaxillary junction

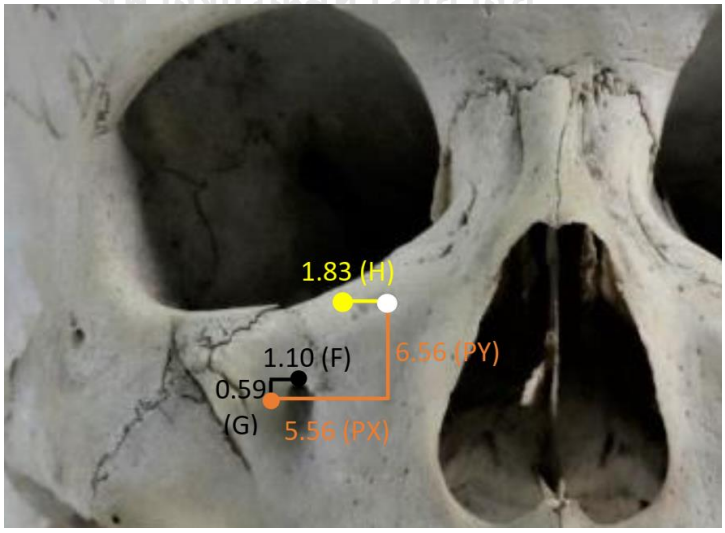

Figure 31. Picture of skull illustrates the mean vertical and horizontal distance between the predicted foramen and the real foramen.

; Black dot= real IOF, Orange dot= predicted IOF, White dot= real AIOF, Yellow dot= predicted AIOF, F= the shortest horizontal distance from the predicted IOF to the real IOF, G= the shortest vertical distance from the predicted IOF to the real IOF, H= the shortest horizontal distance from the predicted AIOF to the real AIOF, PX= horizontal distance between the predicted IOF and the real AIOF, PY= vertical distance between the predicted IOF and the real AIOF
Unit: millimeters

Table 9. Distance A, predicted D, predicted E, F, G, H, I, PX and PY from cadavers (Mean ± SD).

Parameter (mm)	Side			Sex			Total
	Left	Right	p value	Male	Female	p value	
A	47.29 ± 2.32	46.86 ± 2.25	0.117	47.22 ± 2.86	46.91 ± 1.36	0.705	47.07 ± 2.26
Predicted D	29.96 ± 1.47	29.69 ± 1.42	0.117	29.91 ± 1.81	29.72 ± 0.86	0.706	29.82 ± 1.43
Predicted E	24.49 ± 1.20	24.27 ± 1.17	0.117	24.46 ± 1.48	24.30 ± 0.70	0.704	24.38 ± 1.17
F	0.64 ± 1.16	1.56 ± 1.57	0.019*	1.11 ± 1.38	1.09 ± 1.55	0.979	1.10 ± 1.44
G	0.40 ± 1.05	0.79 ± 1.67	0.138	0.41 ± 1.13	0.80 ± 1.65	0.453	0.59 ± 1.39
H	1.83 ± 0.15	-	-	1.72	1.93	-	1.83 ± 0.15
I	0	-	-	0	0	-	0
PX	5.56 ± 0.81	-	-	6.13	4.99	-	5.56 ± 0.81
PY	6.56 ± 0.68	-	-	6.08	7.04	-	6.56 ± 0.68

A= distance from ANS to the lowest point of the zygomaticomaxillary junction, F= the shortest horizontal distance from the predicted IOF to the real IOF, G= the shortest vertical distance from the predicted IOF to the real IOF, H= the shortest horizontal distance from the predicted AIOF to the real AIOF, I= the shortest vertical distance from the predicted AIOF to the real AIOF, Predicted D= average distance A multiplied with the average ratio D:A (63.35%), Predicted E= average distance A multiplied with the average ratio E:A (51.8%), PX= horizontal distance between the predicted IOF and the real AIOF, PY= vertical distance between the predicted IOF and the real AIOF
Unit: millimeters
* statistically significant difference between groups

CHAPTER V

Discussion

Localization of IOF is essential to achieve regional anesthesia of the mid-facial region when performing the ION block in several procedures. In addition to IOF, understanding AIOF is also important because the AION emerges from this foramen and it is associated with the ION (15). Numerous studies examined bony and soft tissue landmarks in order to identify the location of IOF and AIOF. These studies observed bony landmarks some of which can be examined on skulls but are difficult to palpate externally on patient's face such as piriform aperture, zygomaticomaxillary suture and frontomaxillary suture (14, 32-35). Some soft tissue landmarks, for example, ala nasi, lateral palpebral commissure and lacrimal caruncle (40, 43, 46, 47, 49) are visible and can be palpated on the face but don't have bony prominence beneath them which might affect in confirming the reference point and might not represent the soft tissue on patient's face due to the change from preservation process. Although some landmarks such as facial midline, anterior nasal spine and infraorbital margin can be studied both in skulls and cadavers, there was no study considering the measurement in both types of specimen. The location of IOF was described to be 8-10 mm below infraorbital margin in the mid-pupillary line (12). However, this distance varied between studies and could range from 3.2-13.2 mm (32). This variation could be from the inconsistency in the exact referencing point chosen for measurement since infraorbital margin is a long curve line.

Besides the description, we aim to determine anatomical landmarks for more precise localization of IOF and AIOF by using easily palpable landmarks both in bone and soft tissue. Therefore, the line between ANS and the lowest point of the zygomaticomaxillary junction (Z) was taken into consideration. ANS and Z were used as reference points because they can be palpated on dry skull which give benefits for the study since obtaining data from skulls is more convenient and a large number of specimens are available. Moreover, they can be identified on cadaveric soft tissue which is more practical and applicable in clinical settings. This study measured the distances from skulls by image analysis which is two-dimensional assessment. Measuring in two dimensions (2D) might be different from three dimensions (3D) since there is the depth in z-axis which can influence the distance between two structures laying in the different plane. However, there were studies proving that the direct measurements of skulls using Vernier caliper and the measurements taken from image analysis were not statistically significant different (80, 81).

In the present study, the prevalence of AIOF was 19.91% in dry skulls and 6.67% in cadavers which were consistent with the systematic review describing that the prevalence of AIOF in skulls and cadavers ranged from 0.8% to 27.3% (16). On the other hand, later studies found higher prevalence which was 32.1% (14) and 35% (61) in dry skulls. These cadaveric results were also inconsistent with later studies which found the frequency of AIOF in cadavers to be 36.7% (15). We found that AIOF was commonly a single foramen. There were double AIOFs in 2.4% of skulls and no triple foramen was found. AIOF located on the left and right side for 53.49% and 46.51%, respectively. Previous studies reported that AIOF was mostly a single foramen (16, 59, 61) and more common on the left side (14, 16, 38, 61, 63-65), similar to our findings. There were 50% of skulls that had bilateral AIOFs in the present study which was higher than previous reports finding that bilateral AIOF ranged from 9.1% to 25% (14, 16, 58, 62). These differences can due to differences in population, race, and sample size.

The observations made in this study were consistent with previous reports regarding that most of the AIOFs located superomedial to IOF (16, 64, 65). However, there were 3 AIOFs located in the inferolateral position which was different from previous studies. The relationship between IOF and AIOF is important in clinical practice because the failure of complete mid-facial anesthesia after performing an adequate ION block could be due to the presence of AIOF and its neurovascular structure. In order to achieve complete nerve block, clinicians might have to find the location of AIOF to perform AION block by palpating from the location of IOF. According to Rai et al. (2013) the mean distance from AIOF to IOF was 9.79 mm (66), whereas, Tezer et al. (2011) found that the mean distance between AIOF and IOF was 3.95 ± 1.6 mm (65). In this study the mean distance from AIOF to IOF in skulls was 6.10 ± 2.20 mm in horizontal and 4.10 ± 2.06 mm in vertical direction. In cadavers, the real AIOF located 5.56 ± 0.81 mm medial and 6.56 ± 0.68 mm superior to the predicted IOF. This information could be useful in failing to achieve complete anesthesia after predicting the location of IOF for ION block and finding AIOF to undergo the AION block might have to be taken in consideration.

Some previous studies measured the distance between IOF and ANS, but the method was different from this study. Agthong et al. (2005) measured the shortest distance from the center of IOF to ANS which was 34.1 ± 0.2 mm on the right side and 34.3 ± 0.2 mm on the left side. The angle between IOF and ANS ranged from 15° to 35° and the average values was 25.1° ± 0.4° on the right side and 26.8° ± 0.4° on the left side (38). Chrconovic et

al. (2011) measured the shortest distance from the medial-inferior wall of IOF to ANS which was 32.38 ± 2.61 mm and found that the angle was 30.54° ± 5.06° on the right and 31.98° ± 5.02° on the left side (34). In order to find the location of IOF with reference to ANS knowing the distance between these structures is not sufficient, the angle between them is also essential to tell the direction of the distance. In practice, measuring the angle between two structures is difficult and inconvenient which might lead to inaccuracy in finding the location of the foramen. This study used two perpendicular distances between IOF and ANS to predict the location of the foramen, so the angle is not need to be considered which is simpler and more accurate in clinical practice. We found that the vertical distance from the middle-upper edge of IOF to line A and the horizontal distance from ANS to the intersecting point of the vertical line with line A were 15.14 ± 1.99 and 29.75 ± 2.32 mm respectively. From these two distances, the shortest distance from the middle-upper edge of IOF to ANS can be determined from calculation. The finding was 33.43 ± 2.39 mm matching closely with previous studies which might be assumed that measuring from IOF to ANS in two directions and measuring the shortest distance with the angle between IOF and ANS represents the identical result.

The measuring method of AIOF was similar with that of IOF. The mean distance from ANS to the intersecting point of the vertical line from the AIOF with line A was 24.41 ± 3.11 mm and the vertical distance from the middle-upper edge of AIOF to line A was 19.34 ± 3.36 mm. The calculated mean shortest distance from the middle-upper edge of AIOF to ANS was 31.38 ± 2.41 mm. Comparing with the results from previous reports, our result was larger than that of Rai et al. (2013) which found that the mean distance on the right and left side was 25.14 ± 1.35 and 26.46 ± 2.53 mm, respectively (66), but within the interquartile range (IQR) of the result of Martin et al. (2017) which was 30.25–36.75 mm on the right and 26.62–32.23 mm on the left (64). The comparison between previous studies with the results in this study is shown in Table 10.

Table 10. Distances from IOF to ANS and from AIOF to IOF and ANS in previous studies compare with current study (Mean ± SD).

Specimen	Authors	Year	IOF to ANS	AIOF to IOF	AIOF to ANS
Dry skulls	Agthong et al. (37)	2005	Rt. 34.1 ± 0.2 ® Lt. 34.3 ± 0.2 ®		
	Chrcanovic et al. (34)	2011	32.38 ± 2.61		14.72 ± 2.02
	Tezer et al. (65)	2011		3.95 ± 1.60	
	Rai et al. (66)	2013		Rt. 9.60 ± 4.57 Lt. 9.98 ± 2.67	Rt. 25.14 ± 1.35 Lt. 26.46 ± 2.53
	Martin-Junior et al. (64)	2017		Rt. 7.68 (1.29–16.76) ¶ Lt. 6.12 (2.54–13.32) ¶	Rt. 32.49 (30.25–36.75) ¶ Lt. 28.60 (26.62–32.23) ¶
	This study	2021	33.43 ± 2.39	6.10 ± 2.20 in horizontal 4.10 ± 2.06 in vertical	31.38 ± 2.41

AIOF= accessory infraorbital foramen, ANS= anterior nasal spine, IOF= infraorbital foramen, Rt= right, Lt= left
Unit: millimeters
¶ median and interquartile range (IQR)
® = mean and standard error of mean

The location of IOF was predicted by using the ratio of distance from ANS to the intersecting point of the vertical line from IOF with line A (distance D) to distance A (D:A) as predicted horizontal distance, and the predicted vertical distance from the middle-upper edge of IOF to line A (distance B). We found that the mean ratio D:A was 63.35 ± 3.9% which was about two-thirds of distance A and predicted B was 15.14 ± 1.99 mm. For localizing AIOF, we used the ratio of the distance from ANS to the intersecting point of the vertical line from AIOF with line A (distance E) to the distance A (E:A) which was 51.8 ± 5.9% or about half of distance A and the predicted vertical distance from the middle-upper edge of AIOF to line A (distance C) which was 19.34 ± 3.36 mm. There was no statistically significant difference between sex and sides, therefore, we can use the same value in both sex and sides. We analyzed an accuracy of our predicting method by confirming the location of IOF and AIOF in cadavers. The results showed that the prediction of IOF was 50% accurate which means the predicted IOF locates within the real IOF. In cadaveric dissection, only 2 AIOFs were identified. Therefore, there might be too little information to draw a conclusion about the predicting method for localization of AIOF.

Our approach provides an easy and accurate way for localizing IOF and AIOF. Clinicians can use this method as an approximation for performing the ION block by palpating bony prominences of ANS at the uppermost part of philtrum at the level of nostrils and Z at the lowest bony prominence of patient's cheek, then drawing the line between these points. Marking at the medial two-thirds of that line and drawing perpendicularly with and above the line at approximately 15 mm, to identify IOF (Figure 31). Like IOF, clinicians can mark the point in the middle of the line between ANS and the lowest bony point of patient's cheek then measure above that point at approximately 19 mm where AIOF is suspected to be (Figure 32). Since the distance of 1–2 mm is too small to allow the clinicians to discriminate the distance by palpation, the value of the ratio and distance can be adjusted for more applicable methods.

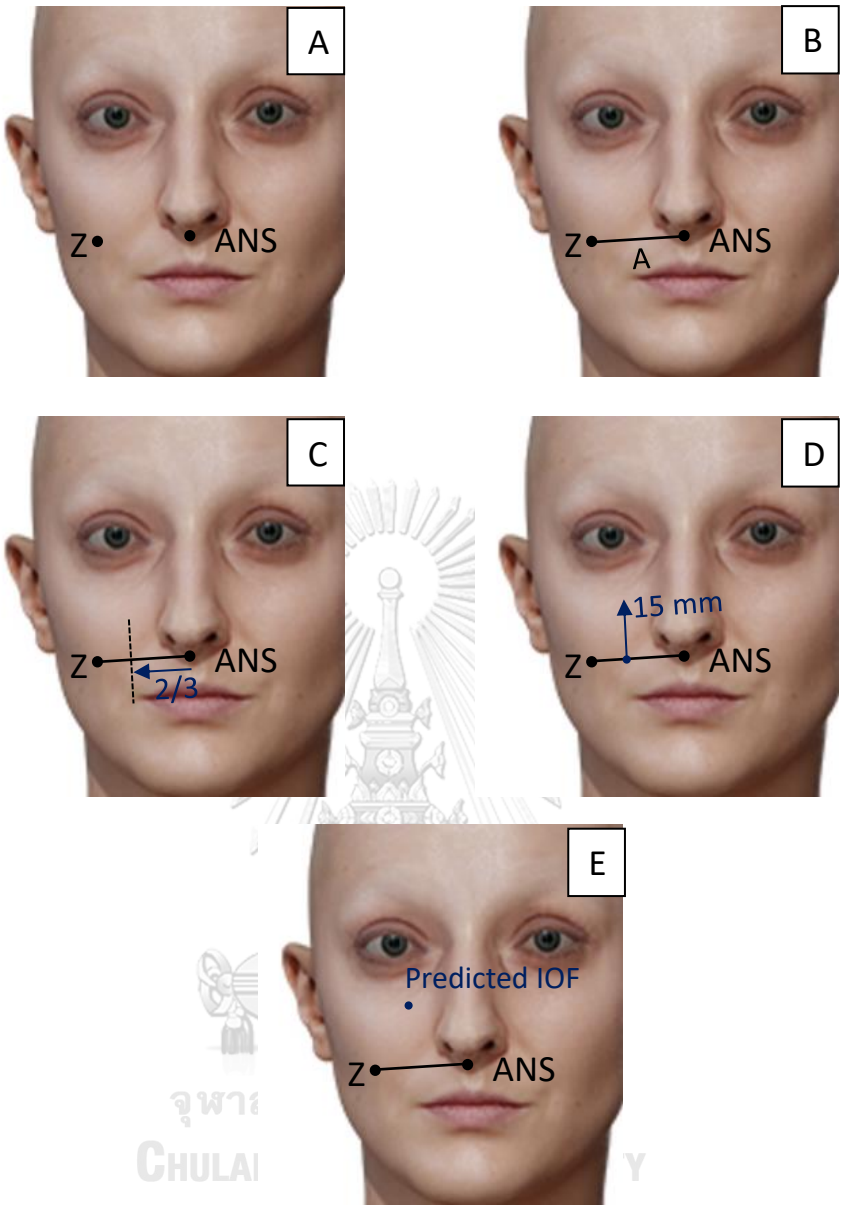

Figure 32. Pictures of female face modified from 3D.SK website (82) describe the predicting method to identify the location of IOF in clinical practice. A. Mark the location of ANS at the uppermost part of philtrum at the level of nostrils and Z at the lowest bony prominence of cheek. B. Draw an imaginary line A between ANS and Z. C. Mark at the medial two-thirds of line A (black dot line) D. Draw perpendicularly with and above line A at approximately 15 mm. E. Mark the location of predicted IOF (dark blue dot).
; A= line from ANS to the lowest point of the zygomaticomaxillary junction, ANS= anterior nasal spine, Z= the lowest point of the zygomaticomaxillary junction

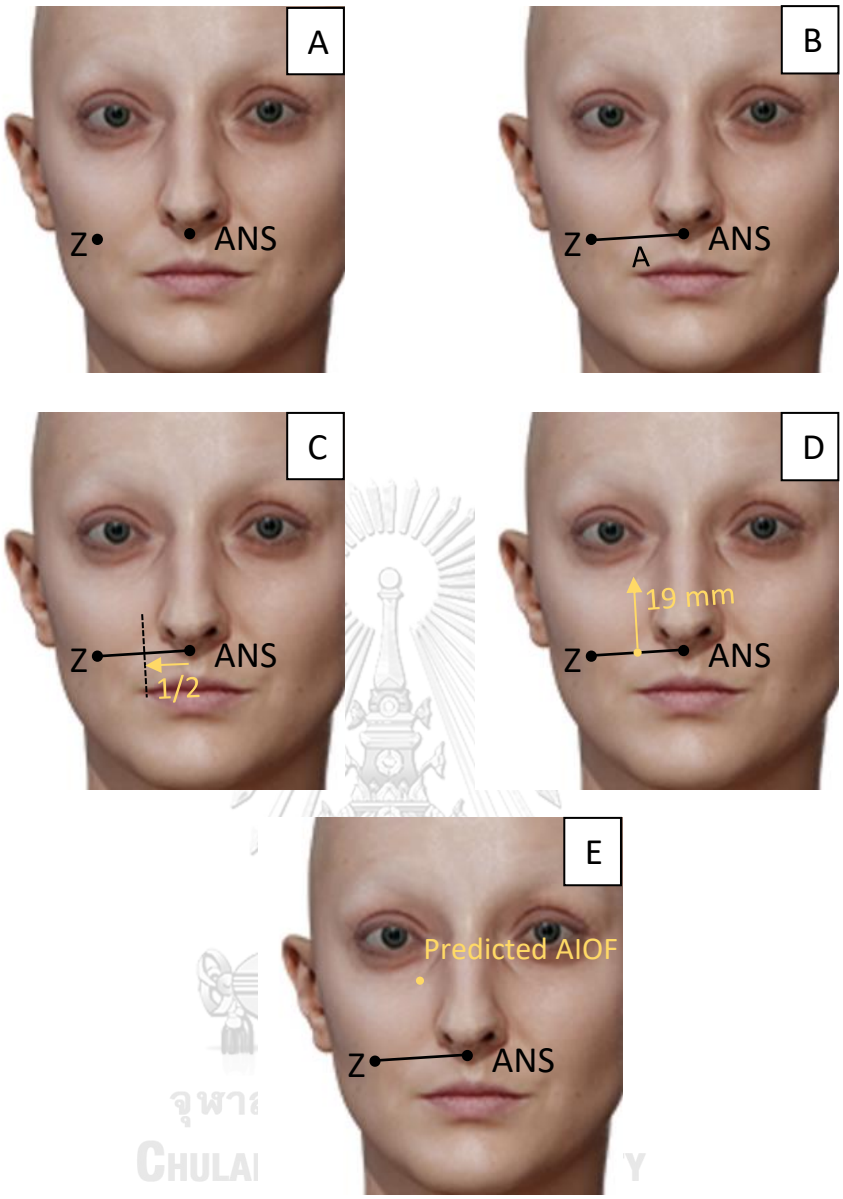

Figure 33. Pictures of female face modified from 3D.SK website (82) describe the predicting method to identify the location of AIOF in clinical practice. A. Mark the location of ANS at the uppermost part of philtrum at the level of nostrils and Z at the lowest bony prominence of cheek. B. Draw an imaginary line A between ANS and Z. C. Mark at the middle of line A (black dot line) D. Draw perpendicularly with and above line A at approximately 19 mm. E. Mark the location of predicted AIOF (yellow dot).
; A= line from ANS to the lowest point of the zygomaticomaxillary junction, ANS= anterior nasal spine, Z= the lowest point of the zygomaticomaxillary junction

Limitations

This study has limitations that should be recognized. Though we identified sex of each skull by using sex identification criteria, there is no available record of ethnicity, sex and age of skulls which may affect the evaluated results. The method for localization of AIOF is inconclusive because the number of AIOF found in cadavers is too small to draw a conclusion. Moreover, we could not compare our method with the standard method for identifying IOF in cadavers since an original pupil position in cadavers had changed and could not be identified accurately. For further consideration, investigating an accuracy of this method in patients who underwent the ION block and comparing the results with the standard method should be performed.

Conclusion

The results of this study provide detailed information of IOF and AIOF, their anatomical relationship and generate the predicting method for localization of IOF and AIOF by using ANS and the lowest point of the zygomaticomaxillary junction as reference points. This method approximately had the mean distance error of 1-2 mm which might not be discriminated by palpation and there were 50% of the predicted IOF locating exactly within the real foramen. Therefore, the proposed predicting method could be an alternative approach and useful in performing more effective and safer procedures around mid-facial area.

REFERENCES

1. Elhadi AM, Zaidi HA, Yagmurlu K, Ahmed S, Rhoton AL, Nakaji P, et al. Infraorbital nerve: a surgically relevant landmark for the pterygopalatine fossa, cavernous sinus, and anterolateral skull base in endoscopic transmaxillary approaches. J Neurosurg. 2016;125(6):1460-68.

2. Hu KS, Kwak HH, Song WC, Kang HJ, Kim HC, Fontaine C, et al. Anatomic studies branching patterns of the infraorbital nerve and topography within the infraorbital space. J Craniofac Surg. 2006;17(6):1111-15.

3. Hu KS, Kwak J, Koh KS, Abe S, Fontaine C, Kim HJ. Topographic distribution area of the infraorbital nerve. Surg Radiol Anat. 2007;29(5):383-88.

4. Bösenberg AT, Kimble FW. Infraorbital nerve block in neonates for cleft lip repair: anatomical study and clinical application. Br J Anaesth. 1995;74(5):506-8.

5. Choi H, Jung SH, Hong JM, Joo YH, Kim Y, Hong SH. Effects of bilateral infraorbital and infratrochlear nerve block on emergence agitation after septorhinoplasty: a randomized controlled trial. J Clin Med. 2019;8(6):769.

6. Molliex S, Navez M, Baylot D, Prades JM, Elkhoury Z, Auboyer C. Regional anaesthesia for outpatient nasal surgery. Br J Anaesth. 1996;76(1):151-3.

7. Spinelli G, Rocchetta D, Carnevali G, Valente D, Conti M, Agostini T. Infraorbital nerve block for isolated orbital floor fractures repair: review of 135 consecutive cases. Plast Reconstr Surg Glob Open. 2014;2(1):97.

8. Cok OY, Deniz S, Eker HE, Oguzkurt L, Aribogan A. Management of isolated infraorbital neuralgia by ultrasound-guided infraorbital nerve block with combination of steroid and local anesthetic. J Clin Anesth. 2017;37:146-8.

9. Perloff MD, Chung JS. Urgent care peripheral nerve blocks for refractory trigeminal neuralgia. Am J Emerg Med. 2018;36(11):2058-60.

10. Boselli E, Bouvet L, Augris-Mathieu C, Begou G, Diot-Junique N, Rahali N, et al. Infraorbital and infratrochlear nerve blocks combined with general anaesthesia for outpatient rhinoseptoplasty: a prospective randomised, double-blind, placebo-controlled study. Anaesth Crit Care Pain Med. 2016;35(1):31-6.

11. McAdam D, Muro K, Suresh S. The use of infraorbital nerve block for postoperative pain control after transsphenoidal hypophysectomy. Reg Anesth Pain Med. 2005;30(6):572-3.

12. Blanton PL, Jeske AH. The key to profound local anesthesia: neuroanatomy. J Am Dent Assoc. 2003;134(6):753-60.

13. Pascal J, Charier D, Perret D, Navez M, Auboyer C. Peripheral blocks of trigeminal nerve for facial soft-tissue surgery: learning from failures. Eur J Anaesthesiol. 2005;22(6):480-2.

14. Polo CL, Abdelkarim AZ, Von AT, Lozanoff S. The morphology of the infraorbital nerve and foramen in the presence of an accessory infraorbital foramen. J Craniofac Surg. 2019;30(1):244-53.

15. Iwanaga J, Kikuta S, Kusukawa J, Tomaszewski KA, Walocha JA, Tubbs RS. Anatomic study of accessory infraorbital nerves and foramina: application for a better understanding of complications of Le Fort fractures and osteotomy. J Oral Maxillofac Surg. 2020;78(5):717-23.

16. Hwang K, Lee SJ, Kim SY, Hwang SW. Frequency of existence, numbers, and location of the accessory infraorbital foramen. J Craniofac Surg. 2015;26(1):274-6.

17. Yang HM, Hu KS, Kim HJ. Anatomical and functional consideration of the trigemino-facial nervous communication and facial expresssion muscles. Korean J Phys Anthropol. 2013;26(1):1-12.

18. Shadlinskiy VB, Guseynov BM, Mustafayeva NA. Variants of the infraorbital nerve branching. Morfologiia 2016;150(4):55-8.

19. Nderitu J, Butt F, Saidi H. Variations in emergence and course of the inferior palpebral nerve. Craniomaxillofac Trauma Reconstr. 2014;7(3):233-6.

20. Khemka G, Khemka SG, Gupta SV. Duplicate infraorbital nerve - an uncommon anatomical variation of branch of maxillary nerve. Int J Sci Res. 2019;8(4):5-6.

21. Tubbs RS, Loukas M, May WR, Cohen Gadol AA. A variation of the infraorbital nerve: its potential clinical consequence especially in the treatment of trigeminal neuralgia: case report. Neurosurgery. 2010;67(3).

22. Byrne KM, Raghavendra M. Infraorbital nerve block. Medscape. 2018.

23. Nardi NM, Alvarado AC, Schaefer TJ. Infraorbital nerve block. StatPearls. 2020.

24. Countryman NB, Hanke CW. Practical review of peripheral nerve blocks in dermatologic surgery of the face. Curr Derm Rep. 2012;1(2):49-54.

25. Lynch MT, Syverud SA, Schwab RA, Jenkins JM, Edlich R. Comparison of intraoral and percutaneous approaches for infraorbital nerve block. Acad Emerg Med. 1994;1(6):514-9.

26. Davies T, Karanovic S, Shergill B. Essential regional nerve blocks for the dermatologist: part 1. Clin Exp Dermatol. 2014;39(7):777-84.

27. Markham JW. Sudden loss of vision following alcohol block of the infraorbital nerve. J Neurosurg. 1973;38(5):655.

28. Feriani G, Hatanaka E, Torloni MR, Da Silva EM. Infraorbital nerve block for postoperative pain following cleft lip repair in children. Cochrane Database Syst Rev. 2016;4(4).

29. Jonnavithula N, Bachu D, Sriramoju V, Devraj R, Gunta R, Pisapati M. Effect of infraorbital nerve block on postoperative pain and 30-day morbidity at the donor site in buccal mucosal graft urethroplasty. J Anaesthesiol Clin Pharmacol. 2019;35(1):114-8.

30. Kim KS, Lee WS, Cho H, Shim SM, Kwak S, Ji SY, et al. Introduction of pulsed radiofrequency cautery in infraorbital nerve block method for postoperative pain management of trauma-induced zygomaticomaxillary complex fracture reduction. J Pain Res. 2019;12:1871-6.

31. Mahli A, Coskun D. Neurolysis for treatment of infraorbital neuropathy. Case Rep Med. 2017;2017.

32. Gupta T. Localization of important facial foramina encountered in maxillo-facial surgery. Clin Anat. 2008;21(7):633-40.

33. Aggarwal A, Kaur H, Gupta T, Tubbs RS, Sahni D, Batra YK, et al. Anatomical study of the infraorbital foramen: a basis for successful infraorbital nerve block. Clin Anat. 2015;28(6):753-60.

34. Chrcanovic BR, Abreu MHNG, Custódio ALN. A morphometric analysis of supraorbital and infraorbital foramina relative to surgical landmarks. Surg Radiol Anat. 2011;33(4):329-35.

35. Kazkayasi M, Ergin A, Ersoy M, Bengi O, Tekdemir I, Elhan A. Certain anatomical relations and the precise morphometry of the infraorbital foramen–canal and groove:

an anatomical and cephalometric study. Laryngoscope. 2001;111(4):609-14.

36. Masabni O, Ahmad M. Infraorbital foramen and pterygopalatine fossa location in dry skulls: anatomical guidelines for local anesthesia. Anat Res Int. 2017;2017.

37. Abed SF, Shams PN, Shen S, Adds PJ, Uddin JM. Morphometric and geometric anatomy of the Caucasian orbital floor. Orbit. 2011;30(5):214-20.

38. Agthong S, Huanmanop T, Chentanez V. Anatomical variations of the supraorbital, infraorbital, and mental foramina related to gender and side. J Oral Maxillofac Surg. 2005;63(6):800-4.

39. Aziz SR, Marchena JM, Puran A. Anatomic characteristics of the infraorbital foramen: a cadaver study. J Oral Maxillofac Surg. 2000;58(9):992-6.

40. Ercikti N, Apaydin N, Kirici Y. Location of the infraorbital foramen with reference to soft tissue landmarks. Surg Radiol Anat. 2017;39(1):11-5.

41. Rahman M, Richter EO, Osawa S, Rhoton AL. Anatomic study of the infraorbital foramen for radiofrequency neurotomy of the infraorbital nerve. Neurosurgery. 2009;64(5):423-7.

42. Zhang KR, Blandford AD, Hwang CJ, Perry JD. Anatomic variations of the infraorbital foramen in Caucasian versus African American skulls. Ophthalmic Plast Reconstr Surg. 2019;35(1):25-8.

43. Shin KJ, Shin HJ, Lee SH. Location of the infraorbital foramen with reference to soft tissue landmarks for regional nerve blocks during midface surgery. Clin Anat. 2020;33(8):1159-63.

44. Levine MR, Allen RC. Manual of oculoplastic surgery. 5th ed. New York: Springer; 2018.

45. Lee JH, Hong G. Definitions of groove and hollowness of the infraorbital region and clinical treatment using soft-tissue filler. Arch Plast Surg. 2018;45(3):214-21.

46. Takahashi Y, Kakizaki H, Nakano T. Infraorbital foramen: horizontal location in relation to ala nasi. Ophthalmic Plast Reconstr Surg. 2011;27(4):295-7.

47. Song WC, Kim SH, Paik DJ, Han SH, Hu KS, Kim HJ, et al. Location of the infraorbital and mental foramen with reference to the soft-tissue landmarks. Plast Reconstr Surg. 2007;120(5):1343-7.

48. Liu DN, Guo JL, Luo Q, Tian Y, Xia CL, Li YQ, et al. Location of supraorbital

foramen/notch and infraorbital foramen with reference to soft- and hard-tissue landmarks. J Craniofac Surg. 2011;22(1):293-6.

49. Zheng WX, Guo JL, Song BX, Liu XL, Lv DL, Tian Y, et al. Location of the supraorbital and infraorbital foramen with references to the soft tissue landmarks in a Chinese population. J Craniofac Surg. 2012;23(4):1154-5.

50. Apinhasmit W, Chompoopong S, Methathrathip D, Sansuk R, Phetphunphiphat W. Supraorbital notch/foramen, infraorbital foramen and mental foramen in Thais: anthropometric measurements and surgical relevance. J Med Assoc Thai. 2006;89(5):675-82.

51. Cheng AC, Lucas PW, Yuen HK, Lam DS, So KF. Surgical anatomy of the Chinese orbit. Ophthalmic Plast Reconstr Surg. 2008;24(2):136-41.

52. Chung MS, Kim HJ, Kang HS, Chung IH. Locational relationship of the supraorbital notch or foramen and infraorbital and mental foramina in Koreans. Acta Anat 1995;154(2):162-6.

53. Hassanali J, Ongeti K, J O, Saidi H. Biometric features of facial foramina in adult Kenyan skulls. Eur J Anat. 2008;12:89-95.

54. Hindy AM, Raouf FA. A study of infraorbital foramen, canal and nerve in adult Egyptians. Egypt Dent J. 1993;39(4):573-80.

55. Karakas P, Bozkir MG, Oguz O. Morphometric measurements from various reference points in the orbit of male Caucasians. Surg Radiol Anat. 2003;24(6):358-62.

56. Rossi M, Ribeiro E, Smith R. Craniofacial asymmetry in development: an anatomical study. Angle Orthod. 2003;73(4):381-5.

57. Sokhn S, Challita R, Challita A, Challita R. The infraorbital foramen in a sample of the Lebanese population: a radiographic study. Cureus. 2019;11(12):6381.

58. Ali IK, Sansare K, Karjodkar FR, Salve P. Cone beam computed tomography assessment of accessory infraorbital foramen and determination of infraorbital foramen position. J Craniofac Surg. 2018;29(2):124-6.

59. Dagistan S, Miloglu O, Altun O, Umar EK. Retrospective morphometric analysis of the infraorbital foramen with cone beam computed tomography. Niger J Clin Pract. 2017;20(9):1053-64.

60. Nanayakkara D, Peiris R, Mannapperuma N, Vadysinghe A. Morphometric analysis

of the infraorbital foramen: the clinical relevance. Anat Res Int. 2016.

61. Nam Y, Bahk S, Eo S. Anatomical study of the infraorbital nerve and surrounding structures for the surgery of orbital floor fractures. J Craniofac Surg. 2017;28(4):1099-104.

62. Shin KJ, Lee SH, Park MG, Shin HJ, Lee AG. Location of the accessory infraorbital foramen with reference to external landmarks and its clinical implications. Sci Rep. 2020;10(1):8566.

63. Gour K, Nair S, Trivedi G, Gupta SD. Anthropometric measurements of infraorbital foramen in dried human skulls. Int J Biol Med Res. 2012;3(3):2003-6.

64. Martins JPA, Rodrigues CP, De Maria ML, Nogueira LM, Silva JH, Silva MR. Analysis of anatomical characteristics and morphometric aspects of infraorbital and accessory infraorbital foramina. J Craniofac Surg. 2017;28(2):528-33.

65. Tezer M, Ozturk A, Akgül M, Gayretli Ö, Kale A. Anatomic and morphometric features of the accessory infraorbital foramen. J Morphol Sci. 2011;28:95-7.

66. Rai AR, Rai R, Vadgaonkar R, Madhyastha S, Rai RK, Alva D. Anatomical and morphometric analysis of accessory infraorbital foramen. J Craniofac Surg. 2013;24(6):2124-26.

67. Rusu MC, Sandulescu M, Carstocea L. False and true accessory infraorbital foramina, and the infraorbital lamina cribriformis. Morphologie. 2020;104(344):51-8.

68. Routine stereo microscopes M50, M60 & M80: Leica Microsystems; 2021 [Available from: https://www.leica-microsystems.com/products/stereo-microscopes-macroscopes/p/leica-m80/downloads/.

69. Rogers TL. Sex determination and age estimation: skeletal evidence from St. Thomas' cemetery Belleville Ontario. Hamilton, ON: McMaster University; 1991.

70. Williams BA, Rogers TL. Evaluating the accuracy and precision of cranial morphological traits for sex determination. J Forensic Sci. 2006;51(4):729-35.

71. White TD, Folkens PA. The Human Bone Manual. 1st ed. San Diego: Elsevier Academic; 2005.

72. Nanda SK, Sassouni V. Planes of reference in roentgenographic cephalometry. Angle Orthod. 1965;35(4):311-9.

73. บำรุงศักดิ์ ธ, ทองอุดมพร อ. จุดและระนาบอ้างอิงจากภาพรังสีกะโหลกศีรษะด้านข้างเพื่อประเมินการ

เคลื่อนที่ของฟันตัดล่าง. Songklanakarin Dent J. 2018;6(1):94-5.

74. Madsen DP, Sampson WJ, Townsend GC. Craniofacial reference plane variation and natural head position. Eur J Orthod. 2008;30(5):532-40.

75. Moorrees C, Kean M. Natural head position, a basic consideration in the interpretation of cephalometric radiographs. Am J Phys Anthropol. 1958;16:213-34.

76. Naini FB. The Frankfort plane and head positioning in facial aesthetic analysis--the perpetuation of a myth. JAMA Facial Plast Surg. 2013;15(5):333-4.

77. Shetty D, Bagga D, Goyal S, Sharma P. A cephalometric study of various horizontal reference planes in natural head position. J Indian Orthod Soc. 2013;47:143-7.

78. Cheng Y, Leow WK, Lim TC. Automatic identification of Frankfurt plane and mid-sagittal plane of skull. 2012 IEEE Workshop on the Applications of Computer Vision (WACV); Breckenridge, CO USA: IEEE; 2012. p. 233-8.

79. Garson JG. The Frankfort craniometric agreement: with critical remarks thereon. JSTOR. 1885;14:64-83.

80. Liu DN, Guo JL, Luo Q, Tian Y, Xia CL, Li YQ, et al. Location of supraorbital foramen/notch and infraorbital foramen with reference to soft- and hard-tissue landmarks. J Craniofac Surg. 2011;22(1):293-6.

81. Mariani TF, Romano PSR. Intra-specific variation and allometry of the skull of Late Cretaceous side-necked turtle Bauruemys elegans (Pleurodira, Podocnemididae) and how to deal with morphometric data in fossil vertebrates. PeerJ. 2017;5:e2890-e.

82. Human photo references and textures for artists 3D.SK; [Available from: https://www.3d.sk/photos/show/id/922983.

APPENDICES

APPENDIX A

Data Record Form

Data from the image analysis are recorded in the form below

Skull No.	Sex	Side	ANS_Z1 (A1)	ANS_Z2 (A2)	IOF_V1 (B1)	IOF_V2 (B2)	IOF_H1 (D1)	IOF_H2 (D2)	AIOF_V1 (C1)	AIOF_V2 (C2)	AIOF_H1 (E1)	AIOF_H2 (E2)	X1	X2	Y1	Y2	Location AIOF to IOF

Data from the cadaveric dissection are recorded in the form below

Cadaver No.	Sex	Side	ANS_Z1	ANS_Z2	ANS_Z_AVR	Predict_ IOF_H	E_IOF_H1 (F1)	E_IOF_H2 (F2)	E_IOF_V1 (G1)	E_IOF_V2 (G2)	Position_IOF

Predict _ AIOF_H	E_AIOF_H1 (H1)	E_AIOF_H2 (H2)	E_AIOF_V1 (I1)	E_AIOF_V2 (I2)	Position_AIOF	PX1	PX2	PY1	PY2	Position_AIOF_IOF

Abbreviation in Appendix A

AIOF_H = E = horizontal distance from ANS to the intersecting point of the vertical line from AIOF with line A

AIOF_V = C = vertical distance from the middle-upper edge of AIOF to line A

ANS_Z = A = distance from anterior nasal spine to the lowest point of the zygomaticomaxillary junction

AVR = Average distance

E_AIOF_H = H = the shortest horizontal distance from the predicted AIOF to the real AIOF

E_AIOF_V = I = the shortest vertical distance from the predicted AIOF to the real AIOF

E_IOF_H = F = the shortest horizontal distance from the predicted IOF to the real IOF

E_IOF_V = G = the shortest vertical distance from the predicted IOF to the real IOF

IOF_H = D = horizontal distance from ANS to the intersecting point of the vertical line from IOF with line A

IOF_V = B = vertical distance from the middle-upper edge of IOF to line A

Position_AIOF = location of the predicted AIOF in relative with the real AIOF

Position_AIOF_IOF = location of the predicted IOF in relative with the real AIOF

Position_IOF = location of the predicted IOF in relative with the real IOF

Predict_ AIOF_H = ANS_Z_AVR multiplied with the average ratio E:A (51.8%)

Predict_ IOF_H = ANS_Z_AVR multiplied with the average ratio D:A (63.35%)

PX = horizontal distance between the predicted IOF and the real AIOF

PY = vertical distance between the predicted IOF and the real AIOF

X = horizontal distance between IOF and AIOF

Y = vertical distance between IOF and AIOF

APPENDIX B
Statistical Analysis of Skulls

Descriptive Analysis of Skulls

Descriptive Statistics

	N	Range	Minimum	Maximum	Mean	Std. Deviation
ANS_Z	432	18.65	37.75	56.40	47.0029	2.94964
IOF_V	432	13.18	8.45	21.63	15.1402	1.99042
IOF_H	432	12.35	24.04	36.39	29.7483	2.31774
AIOF_V	86	18.04	7.98	26.02	19.3423	3.35553
AIOF_H	86	15.18	17.11	32.30	24.4058	3.11259
X	86	11.50	.54	12.04	6.1020	2.19831
Y	86	8.71	.21	8.92	4.1007	2.06442
IOFvsANZ	432	22.16	53.56	75.72	63.3428	3.90155
AIOFvsANZ	86	32.52	35.56	68.08	51.8037	5.90294
Valid N (listwise)	84					

Paired T-Test Analysis in Left and Right Sides of Skulls

Paired Samples Test

		Paired Differences					t	df	Sig. (2-tailed)
		Mean	Std. Deviation	Std. Error Mean	95% Confidence Interval of the Difference Lower	Upper			
Pair 1	Lt_ANS_Z - Rt_ANS_Z	.05947	2.34937	.16023	-.25635	.37529	.371	214	.711
Pair 2	Lt._IOF_V - Rt_IOF_V	-.04106	1.62256	.11066	-.25918	.17706	-.371	214	.711
Pair 3	Lt_IOF_H - Rt_IOF_H	.11345	2.35620	.16069	-.20329	.43019	.706	214	.481
Pair 4	Lt_AIOF_V - Rt_AIOF_V	.76979	2.37494	.57601	-.45129	1.99088	1.336	16	.200
Pair 5	Lt_AIOF_H - Rt_AIOF_H	.54000	3.09787	.75134	-1.05278	2.13278	.719	16	.483
Pair 6	Lt_X - Rt_X	.11365	2.24717	.54502	-1.04174	1.26903	.209	16	.837
Pair 7	Lt_Y - Rt_Y	.67924	2.16360	.52475	-.43318	1.79165	1.294	16	.214
Pair 8	Lt_IOFvsANZ - Rt_IOFvsANZ	.11547	4.82334	.32743	-.52989	.76084	.353	216	.725
Pair 9	Lt_AIOFvsANZ - Rt_AIOFvsANZ	.48372	6.21931	1.50841	-2.71396	3.68140	.321	16	.753

Independent T-Test Analysis in Male and Female Skulls

Independent Samples Test

		Levene's Test for Equality of Variances		t-test for Equality of Means						
									95% Confidence Interval of the Difference	
		F	Sig.	t	df	Sig. (2-tailed)	Mean Difference	Std. Error Difference	Lower	Upper
ANS_Z	Equal variances assumed	.007	.933	5.148	430	.000	1.56176	.30338	.96547	2.15805
	Equal variances not assumed			5.235	241.768	.000	1.56176	.29830	.97415	2.14937
IOF_V	Equal variances assumed	.407	.524	.624	430	.533	.13149	.21084	-.28291	.54590
	Equal variances not assumed			.603	216.722	.547	.13149	.21820	-.29858	.56157
IOF_H	Equal variances assumed	.096	.757	4.379	430	.000	1.05237	.24032	.58002	1.52472
	Equal variances not assumed			4.323	226.638	.000	1.05237	.24342	.57272	1.53201
AIOF_V	Equal variances assumed	.301	.585	.662	84	.510	.52347	.79047	-1.04847	2.09541
	Equal variances not assumed			.609	39.815	.546	.52347	.85979	-1.21449	2.26143
AIOF_H	Equal variances assumed	1.083	.301	.893	84	.374	.65344	.73169	-.80160	2.10848
	Equal variances not assumed			.958	56.330	.342	.65344	.68201	-.71261	2.01949
X	Equal variances assumed	2.637	.108	.754	84	.453	.39011	.51747	-.63893	1.41915
	Equal variances not assumed			.855	64.718	.396	.39011	.45641	-.52148	1.30170
Y	Equal variances assumed	4.776	.032	-.173	84	.863	-.08449	.48750	-1.05394	.88497
	Equal variances not assumed			-.197	64.836	.845	-.08449	.42967	-.94264	.77367
IOFvsANZ	Equal variances assumed	1.611	.205	.438	430	.662	.18093	.41337	-.63155	.99341
	Equal variances not assumed			.454	253.305	.650	.18093	.39821	-.60330	.96516
AIOFvsANZ	Equal variances assumed	1.828	.180	-.624	84	.534	-.86826	1.39098	-3.63438	1.89785
	Equal variances not assumed			-.698	62.566	.488	-.86826	1.24353	-3.35359	1.61706

Intraclass Correlation Coefficient

ANS_Z1 and ANS_Z2

Intraclass Correlation Coefficient

	Intraclass Correlation[b]	95% Confidence Interval		F Test with True Value 0			
		Lower Bound	Upper Bound	Value	df1	df2	Sig
Single Measures	.997[a]	.997	.998	768.784	433	433	.000
Average Measures	.999[c]	.998	.999	768.784	433	433	.000

Two-way mixed effects model where people effects are random and measures effects are fixed.

a. The estimator is the same, whether the interaction effect is present or not.

b. Type A intraclass correlation coefficients using an absolute agreement definition.

c. This estimate is computed assuming the interaction effect is absent, because it is not estimable otherwise.

IOF_V1 and IOF_V2

Intraclass Correlation Coefficient

	Intraclass Correlation[b]	95% Confidence Interval		F Test with True Value 0			
		Lower Bound	Upper Bound	Value	df1	df2	Sig
Single Measures	.998[a]	.998	.999	1247.733	433	433	.000
Average Measures	.999[c]	.999	.999	1247.733	433	433	.000

Two-way mixed effects model where people effects are random and measures effects are fixed.

a. The estimator is the same, whether the interaction effect is present or not.

b. Type A intraclass correlation coefficients using an absolute agreement definition.

c. This estimate is computed assuming the interaction effect is absent, because it is not estimable otherwise.

IOF_H1 and IOF_H2

Intraclass Correlation Coefficient

	Intraclass Correlation[b]	95% Confidence Interval		F Test with True Value 0			
		Lower Bound	Upper Bound	Value	df1	df2	Sig
Single Measures	.995[a]	.994	.996	388.007	433	433	.000
Average Measures	.997[c]	.997	.998	388.007	433	433	.000

Two-way mixed effects model where people effects are random and measures effects are fixed.

a. The estimator is the same, whether the interaction effect is present or not.

b. Type A intraclass correlation coefficients using an absolute agreement definition.

c. This estimate is computed assuming the interaction effect is absent, because it is not estimable otherwise.

AIOF_V1 and AIOF_V2

Intraclass Correlation Coefficient

	Intraclass Correlation[b]	95% Confidence Interval		F Test with True Value 0			
		Lower Bound	Upper Bound	Value	df1	df2	Sig
Single Measures	.999[a]	.999	1.000	3146.825	85	85	.000
Average Measures	1.000[c]	1.000	1.000	3146.825	85	85	.000

Two-way mixed effects model where people effects are random and measures effects are fixed.

a. The estimator is the same, whether the interaction effect is present or not.

b. Type A intraclass correlation coefficients using an absolute agreement definition.

c. This estimate is computed assuming the interaction effect is absent, because it is not estimable otherwise.

AIOF_H1 and AIOF_H2

Intraclass Correlation Coefficient

	Intraclass Correlation[b]	95% Confidence Interval		F Test with True Value 0			
		Lower Bound	Upper Bound	Value	df1	df2	Sig
Single Measures	.987[a]	.980	.991	149.835	85	85	.000
Average Measures	.993[c]	.990	.996	149.835	85	85	.000

Two-way mixed effects model where people effects are random and measures effects are fixed.

a. The estimator is the same, whether the interaction effect is present or not.

b. Type A intraclass correlation coefficients using an absolute agreement definition.

c. This estimate is computed assuming the interaction effect is absent, because it is not estimable otherwise.

X1 and X2

Intraclass Correlation Coefficient

	Intraclass Correlation[b]	95% Confidence Interval		F Test with True Value 0			
		Lower Bound	Upper Bound	Value	df1	df2	Sig
Single Measures	.993[a]	.989	.995	286.869	85	85	.000
Average Measures	.996[c]	.995	.998	286.869	85	85	.000

Two-way mixed effects model where people effects are random and measures effects are fixed.

a. The estimator is the same, whether the interaction effect is present or not.

b. Type A intraclass correlation coefficients using an absolute agreement definition.

c. This estimate is computed assuming the interaction effect is absent, because it is not estimable otherwise.

Y1 and Y2

Intraclass Correlation Coefficient

	Intraclass Correlation[b]	95% Confidence Interval		F Test with True Value 0			
		Lower Bound	Upper Bound	Value	df1	df2	Sig
Single Measures	.995[a]	.992	.997	395.832	85	85	.000
Average Measures	.997[c]	.996	.998	395.832	85	85	.000

Two-way mixed effects model where people effects are random and measures effects are fixed.

a. The estimator is the same, whether the interaction effect is present or not.

b. Type A intraclass correlation coefficients using an absolute agreement definition.

c. This estimate is computed assuming the interaction effect is absent, because it is not estimable otherwise.

Abbreviation in Appendix B

AIOF_H = horizontal distance from ANS to the intersecting point of the vertical line from AIOF with line A

AIOF_V = vertical distance from the middle-upper edge of AIOF to line A

AIOFvsANZ = percentage of the ratio of distance AIOF_H to distance ANS_Z

ANS_Z = distance from anterior nasal spine to the lowest point of the zygomaticomaxillary junction

IOF_H = horizontal distance from ANS to the intersecting point of the vertical line from IOF with line A

IOF_V = vertical distance from the middle-upper edge of IOF to line A

IOFvsANZ = percentage of the ratio of distance IOF_H to distance ANS_Z

X = horizontal distance between IOF and AIOF

Y = vertical distance between IOF and AIOF

APPENDIX C
Statistical Analysis of Cadavers

Descriptive Analysis of Cadavers

Descriptive Statistics

	N	Range	Minimum	Maximum	Mean	Std. Deviation
ANS_Z	30	8.18	43.13	51.31	47.0732	2.25518
Predict_IOF_H	30	5.18	27.32	32.50	29.8213	1.42792
Predict_AIOF_H	30	4.24	22.34	26.58	24.3840	1.16847
E_IOF_H	30	3.98	.00	3.98	1.0990	1.43525
E_IOF_V	30	5.03	.00	5.03	.5932	1.38587
E_AIOF_H	2	.21	1.72	1.93	1.8250	.14849
E_AIOF_V	2	.00	.00	.00	.0000	.00000
PX	2	1.14	4.99	6.13	5.5600	.80610
PY	2	.96	6.08	7.04	6.5600	.67882
Valid N (listwise)	2					

Paired T-Test Analysis in Left and Right Sides of Cadavers

Paired Samples Test

		Paired Differences					t	df	Sig. (2-tailed)
		Mean	Std. Deviation	Std. Error Mean	95% Confidence Interval of the Difference Lower	Upper			
Pair 1	Lt_ANS_Z - Rt_ANS_Z	.42367	.98367	.25398	-.12107	.96840	1.668	14	.117
Pair 2	Lt_Predict_IOF_H - Rt_Predict_IOF_H	.26933	.62426	.16118	-.07637	.61504	1.671	14	.117
Pair 3	Lt_Predict_AIOF_H - Rt_Predict_AIOF_H	.22000	.50987	.13165	-.06236	.50236	1.671	14	.117

Paired Samples Test

		Paired Differences					t	df	Sig. (2-tailed)
		Mean	Std. Deviation	Std. Error Mean	95% Confidence Interval of the Difference Lower	Upper			
Pair 1	Lt_E_IOF_H - Rt_E_IOF_H	-.92067	1.34606	.34755	-1.66609	-.17524	-2.649	14	.019
Pair 2	Lt_E_IOF_V - Rt_E_IOF_V	-.38900	.95706	.24711	-.91900	.14100	-1.574	14	.138

Independent T-Test Analysis in Male and Female Cadavers

Independent Samples Test

		Levene's Test for Equality of Variances		t-test for Equality of Means						
									95% Confidence Interval of the Difference	
		F	Sig.	t	df	Sig. (2-tailed)	Mean Difference	Std. Error Difference	Lower	Upper
ANS_Z	Equal variances assumed	17.067	.000	.368	28	.716	.30795	.83790	-1.40841	2.02431
	Equal variances not assumed			.384	22.027	.705	.30795	.80212	-1.35543	1.97132
Predict_IOF_H	Equal variances assumed	16.952	.000	.366	28	.717	.19402	.53055	-.89276	1.28080
	Equal variances not assumed			.382	22.041	.706	.19402	.50792	-.85923	1.24726
Predict_AIOF_H	Equal variances assumed	17.006	.000	.369	28	.715	.16018	.43413	-.72910	1.04945
	Equal variances not assumed			.385	22.045	.704	.16018	.41562	-.70166	1.02202

Independent Samples Test

		Levene's Test for Equality of Variances		t-test for Equality of Means						
									95% Confidence Interval of the Difference	
		F	Sig.	t	df	Sig. (2-tailed)	Mean Difference	Std. Error Difference	Lower	Upper
E_IOF_H	Equal variances assumed	.717	.404	.027	28	.979	.01420	.53454	-1.08076	1.10915
	Equal variances not assumed			.026	26.284	.979	.01420	.53892	-1.09299	1.12138
E_IOF_V	Equal variances assumed	2.499	.125	-.760	28	.453	-.38848	.51091	-1.43503	.65806
	Equal variances not assumed			-.742	22.546	.466	-.38848	.52387	-1.47340	.69644
E_AIOF_H	Equal variances assumed	.	.	.	0	.	-.21000	.	.	.
	Equal variances not assumed			.	.	.	-.21000	.	.	.
E_AIOF_V	Equal variances assumed	.	.	.	0	.	.00000	.	.	.
	Equal variances not assumed			.	.	.	.00000	.	.	.
PX	Equal variances assumed	.	.	.	0	.	1.14000	.	.	.
	Equal variances not assumed			.	.	.	1.14000	.	.	.
PY	Equal variances assumed	.	.	.	0	.	-.96000	.	.	.
	Equal variances not assumed			.	.	.	-.96000	.	.	.

Abbreviation in Appendix C

ANS_Z = distance from anterior nasal spine to the lowest point of the zygomaticomaxillary junction

E_AIOF_H = the shortest horizontal distance from the predicted AIOF to the real AIOF

E_AIOF_V = the shortest vertical distance from the predicted AIOF to the real AIOF

E_IOF_H = the shortest horizontal distance from the predicted IOF to the real IOF

E_IOF_V = the shortest vertical distance from the predicted IOF to the real IOF

Predict_AIOF_H = average distance A multiplied with the average ratio E:A (51.8%)

Predict_IOF_H = average distance A multiplied with the average ratio D:A (63.35%)

PX = horizontal distance between the predicted IOF and the real AIOF

PY = vertical distance between the predicted IOF and the real AIOF

VITA

NAME	Jiraporn Suntiruamjairucksa
DATE OF BIRTH	02 April 1995
PLACE OF BIRTH	Bangkok, Thailand
INSTITUTIONS ATTENDED	Faculty of Medicine, Chulalongkorn University
HOME ADDRESS	79/186, The Master Sathorn Executive, Krungthonburi Road, Klongtonsai, Klongsarn, Bangkok Thailand, 10600